

# ETS1 regulates the expression of *ATXN2*

Daniel R. Scoles\*, Lance T. Pflieger, Khanh K. Thai, Stephen T. Hansen, Warunee Dansithong and Stefan-M. Pulst

Department of Neurology, University of Utah, 175 North Medical Center Drive East, 5th Floor, Salt Lake City, UT 84132, USA

Received June 15, 2012; Revised June 15, 2012; Accepted August 15, 2012

**Spinocerebellar ataxia type 2 (SCA2) is an autosomal dominant disorder caused by the expansion of a CAG tract in the *ATXN2* gene. The SCA2 phenotype is characterized by cerebellar ataxia, neuropathy and slow saccades. SCA2 foreshortens life span and is currently without symptomatic or disease-modifying treatments. Identifying function-specific therapeutics for SCA2 is problematic due to the limited knowledge of *ATXN2* function. As SCA2 is likely caused by a gain-of-toxic or gain-of-normal function like other polyglutamine disorders, targeting *ATXN2* expression may represent a valid therapeutic approach. This study characterized aspects of *ATXN2* expression control using an *ATXN2* promoter-luciferase (*luc*) reporter construct. We verified the fidelity of construct expression by generating transgenic mice expressing the reporter construct. High reporter expression was seen in the cerebellum and olfactory bulb *in vivo* but there was relatively low expression in other tissues, similar to the expression of endogenous ataxin-2. We verified the second of two possible start codons as the functional start codon in *ATXN2*. By evaluating deletions in the *ATXN2* promoter, we identified an E-twenty six (ETS)-binding site required for *ATXN2* expression. We verified that endogenous ETS1 interacted with the *ATXN2* promoter by an electromobility supershift assay and chromatin immunoprecipitation polymerase chain reaction. ETS1 overexpression increased *ATXN2-luc* (*ATXN2-luciferase*) as well as endogenous *ATXN2* expression. Deletion of the putative ETS1-binding site abrogated the effects on the expression of *ATXN2-luc*. A dominant negative ETS1 and an ETS1 short-hairpin RNA both reduced *ATXN2-luc* expression. Our study broadens the understanding on the transcriptional control of *ATXN2* and reveals specific regulatory features of the *ATXN2* promoter that can be exploited therapeutically.**

## INTRODUCTION

Spinocerebellar ataxia type 2 (SCA2) is an autosomal dominant neurodegenerative disease characterized by progressive functional and cell loss of neurons in the cerebellum, brain stem and spinal cord. The cause of SCA2 is CAG expansion in the *ATXN2* gene resulting in polyglutamine (polyQ) expansion in the ataxin-2 protein. Patients with SCA2 are characterized by progressive cerebellar ataxia, slow saccadic eye movements and other neurologic features such as neuropathy (1). Moderate CAG expansion in the *ATXN2* gene is also associated with parkinsonism or amyotrophic lateral sclerosis (ALS) indistinguishable from the idiopathic forms of these diseases (2–6).

The pathogenic functions of polyQ disease proteins that occur with polyQ expansion may be attributed to the gain of toxicity associated with the development of intranuclear inclusion bodies or with soluble toxic oligomers (7). While SCA2

patient brains are characterized by loss of Purkinje cells, SCA2 Purkinje cells lack inclusion bodies indicating polyQ-expanded ataxin-2 may cause toxicity that is unrelated to inclusion body formation (8). Functions gained in polyQ-expanded ataxin-2 may include anomalous accumulation in Golgi bodies (9), gain-of-normal functions (10) and sequestering of transcription factors (TFs) and glyceraldehyde-3-phosphate dehydrogenase like for other polyQ proteins (11–13). Some normal functions of ataxin-2 have been characterized. Ataxin-2 is present in stress granules and P-bodies suggesting functions in sequestering mRNAs and protein translation regulation during stress (14). Ataxin-2 overexpression interfered with the P-body assembly, while underexpression interfered with stress granule assembly (14). Interactions with polyA-binding protein 1, the RNA splicing factor A2BP1/Fox1 and polyribosomes further support roles for ataxin-2 in RNA metabolism (15–17). Ataxin-2 is a regulator

\*To whom correspondence should be addressed. Tel: +1 8015852886; Fax: +1 8015816707; Email: daniel.scoles@hsc.utah.edu

of EGF receptor internalization and signaling by the way of its interactions with SRC kinase and the endocytic protein CIN85 (18). Ataxin-2 also interacts with the ALS-related protein TDP-43 in an RNA-dependent manner and familial and sporadic ALS associates with the occurrence of long normal CAG repeat expansion *ATXN2* (5,6).

Mutant ataxin-2 is also an effector of  $\text{Ca}^{2+}$  efflux from the endoplasmic reticulum by binding inositol 1,4,5-triphosphate receptor ( $\text{InsP}_3\text{R}$ ). Greater  $\text{Ca}^{2+}$  efflux was observed in cultures of mouse primary neurons possessing ataxin-2 Q58 than Q22 and the SCA2-related phenotype of ataxin-2 Q58 transgenic mice was resolved with dantrolene, an inhibitor of the ryanodine receptor (19). Previous work by our group also showed that long normal CAG repeats in the *CACNA1A* calcium channel gene lowered SCA2 age of onset (20). Collectively, these findings suggest a functional connection between ataxin-2 and calcium metabolism that with further characterization might be exploited therapeutically for SCA2.

The concept of developing a treatment for SCA2 by reducing total *ATXN2* expression was the primary motivation for this study. Studies in rodents on SCA2 and other polyQ disease genes provided support for this approach. For Huntington's disease, SCA1 and SCA3, reductions in the mutant proteins for these diseases (huntingtin, ataxin-1 and ataxin-3, respectively) resulted in phenotype reversals after phenotype onset in inducible mice (21–23). In a rat model of Machado-Joseph disease, silencing of both the wild-type and mutant ataxin-3 genes improved neuropathology, while allele-specific silencing of just the wild-type ataxin-3 gene did not worsen pathology (24). We also noted no neuropathology in *ATXN2* knockout mice (25). The regulatory features of the *ATXN2* gene remain poorly described. In one study of the *ATXN2* promoter, various regulatory elements including predictions for Sp1-binding sites were identified in the exon 1 region as well as a promoter-localized CpG island (26). Another study demonstrated that the KRAB-containing zinc-finger transcriptional regulator ZBRK1 forms a complex with ataxin-2 that transactivates *ATXN2* (27).

In the present study, we further characterize regulatory features of the *ATXN2* gene by introducing mutational changes in various *ATXN2* promoter-luciferase (*luc*)-*ATXN2*-3'-UTR plasmid constructs, with the purpose to identify regulatory features that might be exploited therapeutically. Deletions in the upstream region and 5'-UTR resulted in the identification of specific regions in *ATXN2* for expression control. Within the 5'-UTR, we identified a 14 bp region required for *ATXN2* expression that spans an 8 bp sequence that has 100% consensus with the E-twenty six (ETS) family TF-binding site. We found that this region directed the regulation of *ATXN2* expression by the TF ETS1. We also characterized the effects of CAG repeat expansion on *ATXN2* expression and the ataxin-2 expression in *ATXN2-luc* (*ATXN2*-luciferase) transgenic mice.

## RESULTS

### Luciferase expression from pGL2-5A3

Our approach to cloning pGL2-5A3 (Fig. 1) involved six steps resulting in various clones with different promoters and polyA features. We conducted luciferase assays comparing among the different plasmids made in this cloning process and

pGL2-5A3, providing insight on the behavior of ataxin-2-luciferase expression from this plasmid (Fig. 1B). Three primary observations were made: first, luciferase expression increased by 2-fold when the pGL2-Enhancer vector provided polyA and the SV40 enhancer sequence was replaced by the *ATXN2*-3'-UTR. This observation indicated that the *ATXN2*-3'-UTR imparts considerable RNA stability, since the vector-encoded SV40 polyA enhancer was designed to increase expression. Second, adding an additional 298 bp of *ATXN2* exon 1 including the second ATG while simultaneously placing the *ATXN2* exon 1 fragment in frame with luciferase, markedly improved expression increasing luciferase activity by 4-fold compared with lack of this fragment. This indicated that the *ATXN2-luc* transcript preferentially utilizes its own ATG over the luciferase ATG. Third, luciferase expression was reduced by 25% when the vector-encoded ATG was mutated to CTG creating a fusion of the ataxin-2 exon 1-encoded protein fragment with luciferase.

### The second ATG in *ATXN2* is the *ATXN2* start codon

In order to understand the relative usage of the two in-frame start codons located in *ATXN2* exon 1, we generated two additional clones of pGL2-5A3, each with one of the codons changed to CTG. Luciferase assays and immunoblotting analysis showed that expression was abolished upon the mutation of the second start codon but not the first (Fig. 1C and D). Thus, the second ATG in the reading frame represents the *ATXN2* start codon. We have never observed by western blotting evidence of two ataxin-2 bands or two ataxin-2-luciferase bands indicative of the utilization of two start codons.

### Effect of CAG expansion on *ATXN2-luc* expression

We evaluated the effect of CAG expansion on *ATXN2* expression, with an experimental design to distinguish between CAG length effects on the *ATXN2* message and the ataxin-2 protein. We did this because we predicted that the CAG repeat length controls *ATXN2* expression, since the CAG repeat is located within a predicted CpG island (26) and because we now localized the start codon to just 15 bp upstream of the repeat (Fig. 1C and D). We observed that addition of a 108 bp fragment just downstream of the single CAG in our plasmid pGL2-5A3 caused a slight decrease in *ATXN2-luc* expression in luciferase assays that, however, was not evident by western blotting (Fig. 2A and B). The 108 bp fragment was added because it harbors CpG island characteristics and therefore may support transcription (26). Increasing the CAG repeat from 1 to 22 or 57 CAGs significantly increased the expression of *ATXN2-luc* in luciferase assays (2.7-fold) and as detected by immunoblotting (4.1-fold; Fig. 2A and B). Further increase in the CAG tract to 102 CAGs resulted in a significant reduction in *ATXN2-luc* expression in luciferase assays and immunoblots (Fig. 2A and B). The length of the CAG tract caused no significant differences in *ATXN2-luc* expression as determined by quantitative polymerase chain reaction (qPCR; Fig. 2C). To support these observations, we conducted two additional western blot experiments with an entirely different set of plasmids with full-length *ATXN2* and varying CAG repeat lengths. The additional set of plasmids included CAG lengths 22, 58

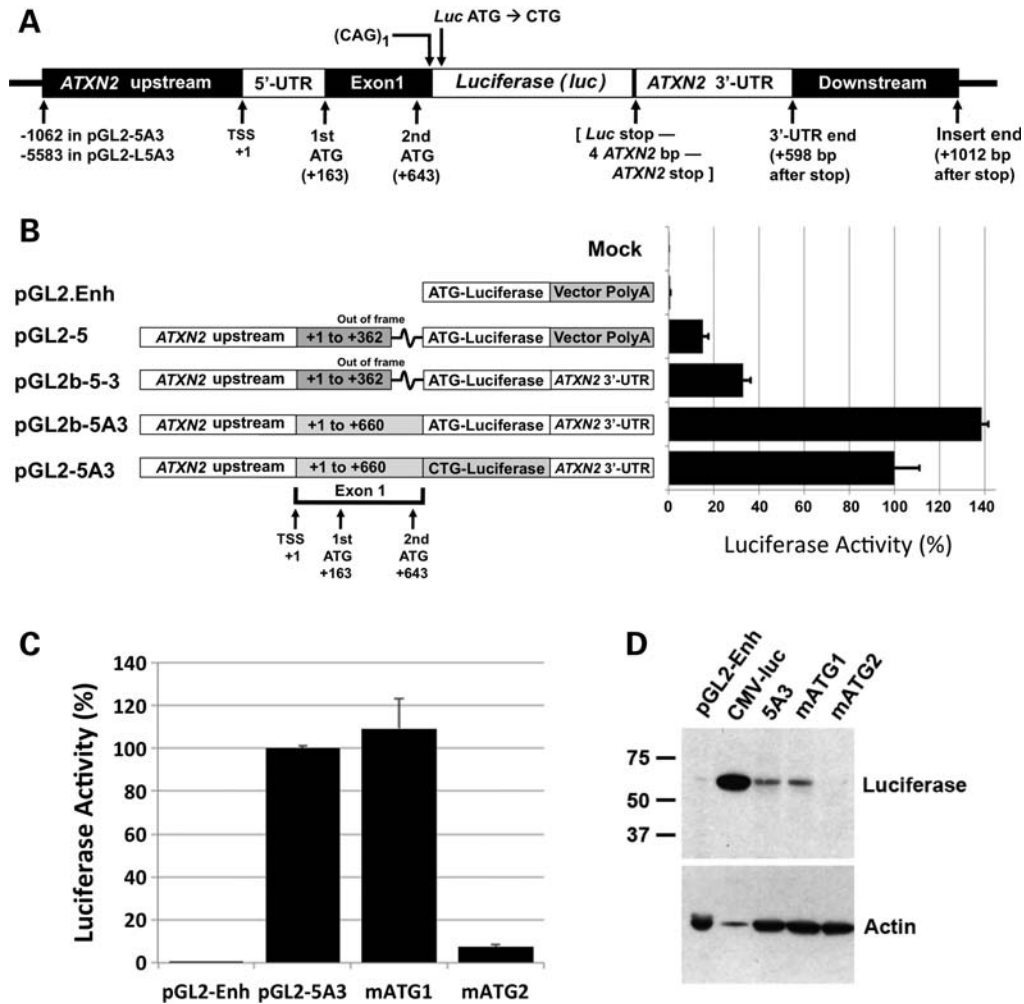


**Figure 1.** Cloning of pGL2-5A3 and evaluation of start codons. (A) Features of pGL2-5A3, the principal clone from which most other constructs in the study were made. pGL2-5A3 includes  $-1062$  to  $+660$  of the *ATXN2* gene ending on the first CAG of the CAG tract followed by an *XhoI* restriction site. The luciferase start codon was mutated to CTG, encoding leucine, so to fuse the ataxin-2 fragment with luciferase. Downstream of the luciferase stop codon is an *AgeI* restriction site followed by 1019 bp of *ATXN2* 3'-UTR and downstream sequence ( $+4098$  to  $+5116$ ). *ATXN2* bp positions are relative to the TSS except as indicated in the figure. (B) Representation of the cloning process from top to bottom, comparing pGL2-5A3 to three of its 'ancestral' plasmids and the vector from which they were made, pGL2.Enhancer (pGL2.Enh). Colored boxes indicate differences among the cloned regions. Note that addition of the 'A' fragment of *ATXN2* exon 1 in pGL2b-5A3 placed the longer exon 1 fragment in frame with luciferase. On the right are the results of assays showing how expression of luciferase differed among these plasmids. Shown are the mean  $\pm$  SD of  $RLU_{firefly}/RLU_{Renilla}$  values from three independent transfections each read in triplicate, expressed as a percentage. (C) Relative use of the two start codons in *ATXN2*. Luciferase assays were conducted to compare expression from pGL2-5A3 with two plasmids where either of the two start codons were mutated to CTG, pGL2-5A3(mATG1) and pGL2-5A3(mATG2). Mutation of the second start codon resulted in nearly complete loss of *ATXN2-luc* expression, while mutation of the first start codon resulted in no expression change. The data shown are for HEK293 cells. The experiment conducted in SH-SY5Y cells showed a nearly identical result. (D) Western blot analysis with anti-luciferase antibody of proteins expressed from pGL2-5A3, pGL2-5A3(mATG1) and pGL2-5A3(mATG2) in HEK293 revealed *ATXN2-luc* proteins of the size predicted for the usage of the second start codon. Note that lane 2 was purposefully underloaded.

and 108, had 4.0 kb of *ATXN2* upstream sequence/native promoter and included a control cytomegalovirus-green fluorescent protein (CMV-GFP) gene encoded on the same plasmids (Fig. 2D). Western blotting demonstrated significantly reduced ataxin-2 expression for CAG108 only (Fig. 2D) and the result was nearly identical to that shown in Fig. 2B.

#### Exogenous *ATXN2-luc* parallels endogenous *ATXN2* expression *in vivo*

We established two lines of transgenic mice carrying the *ATXN2-luc* transgene, designated L74 and L75. We initially

used luciferase assays of excised brain tissues to verify that the *ATXN2-luc* transgene was expressed (data not shown). Both L74 and L75 had the highest expression of *ATXN2-luc* in the cerebellum while low expression was observed in other tissues, including the heart and total brain. Subsequently, we evaluated only line L75 with the highest *ATXN2-luc* expression. qPCR analysis of multiple mice showed uniform *ATXN2-luc* expression relative to mouse *Atxn2* in several tissues, including the total brain, nose, whisker pad, tongue, paw pad, heart, kidney and testis, but high relative expression in the cerebellum and olfactory bulb (OB; Fig. 3A). *in vivo* imaging system (IVIS) imaging of luciferase in whole

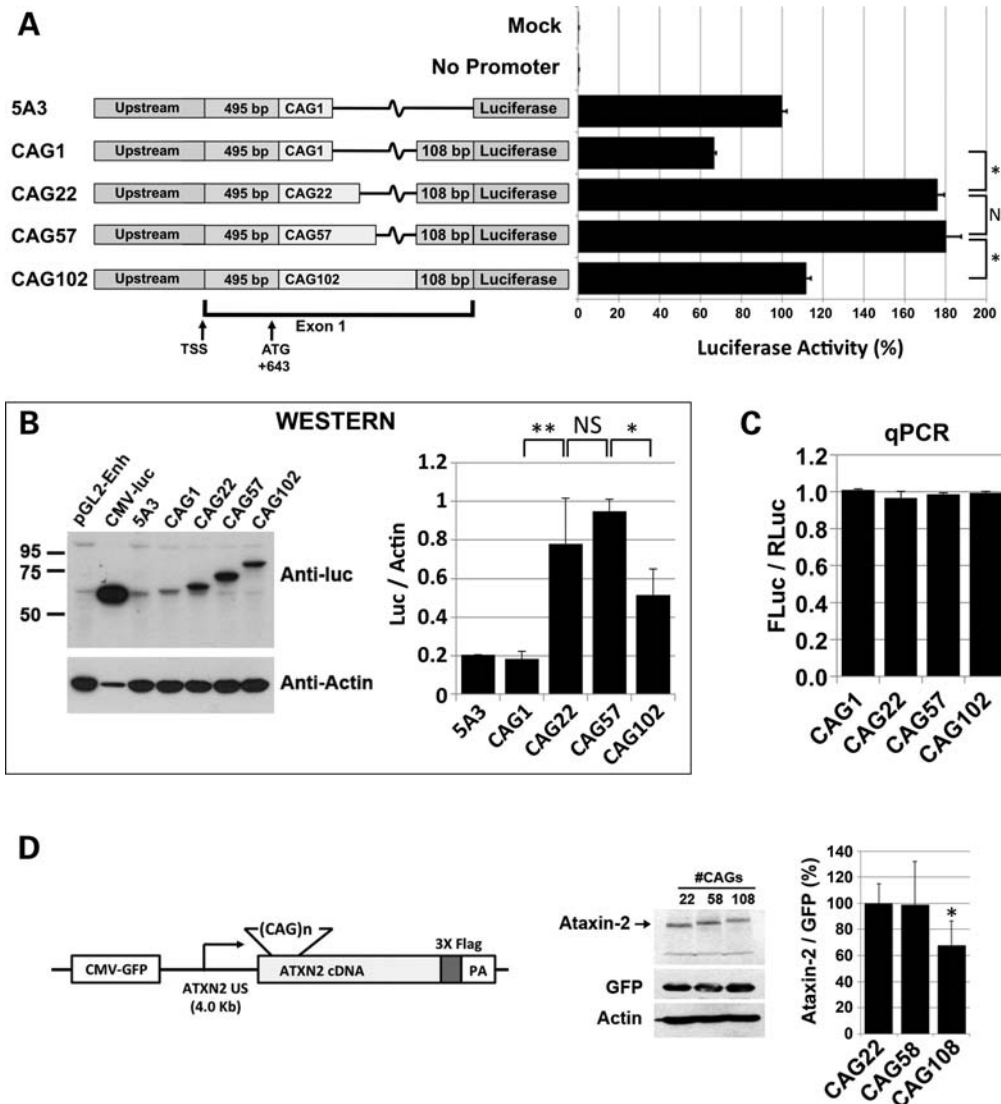


**Figure 2.** Effect of CAG length on *ATXN2* expression. (A) Luciferase assays using *ATXN2-luc* constructs with increasing CAG repeat lengths revealed highest expression for CAG22 and CAG57 and lower expression for longer CAG lengths. All constructs were based on pGL2-5A3. Identical results were obtained when the experiment was repeated using constructs modified to include TK-Renilla cassettes on the same plasmids. (B) Western blot analysis of the constructs in (A) revealed a similar pattern of protein expression to that determined by luciferase assays in (A). Note that lane 2 was purposefully underloaded. (C) qPCR analysis using constructs shown in (A) that were modified to include TK-Renilla cassettes on the same plasmids, showed no changes in the abundances of the *ATXN2-luc* transcript depending upon the CAG length. (D) Constructs expressing full-length *ATXN2* with repeat lengths CAG22, CAG58 and CAG108 including 4 kb *ATXN2* upstream sequence, analyzed by western blotting with anti-FLAG antibody. Like in (A) and (B), the longest repeat (CAG108) reduced *ATXN2* expression. The asterisk indicates a significant difference for CAG108 versus either CAG22 or CAG58 ( $P < 0.05$ , Bonferroni post-test,  $n = 7$  transfections). Expression was relative to GFP encoded on the same plasmid as indicated. Actin is also shown. HEK293 cells (A–C) and SH-SY5Y cells (D).

animals revealed high *ATXN2-luc* expression in the nose (Fig. 3B) which was regularly observed among mice, although by qPCR *ATXN2-luc* expression in the nose was not elevated (Fig. 3A). We also observed high expression in the cauda epididymis (Fig. 3B and Supplementary Material, Fig. S1). Additionally, we observed luciferase signals in whole animals consistent with expression in the cerebellum and OB that were absent in wild-type controls (Fig. 3C). Excised whole brains showed elevated expression in the OB and cerebellum that was more widespread in 2-month-old animals (Fig. 3D) compared with 7-month-old animals (Fig. 3E). We characterized the distribution of *ATXN2* in the OB of wild-type C57Bl/6

mice by indirect immunofluorescent (IF) labeling to verify that *ATXN2-luc* expression in OB was consistent with endogenous *ATXN2* expression. *ATXN2* was strongly expressed in mitral cells and in tufted cells of the glomerular layer (Fig. 3F–L).

#### *ATXN2* promoter deletion and *ATXN2-luc* expression

We performed luciferase assays to compare expression between the pGL2-5A3 plasmid containing *ATXN2* upstream sequence including  $-1062$  bp from the transcription start site (TSS, as defined for ENST00000377617 in the Ensembl Genome Browser, [www.ensembl.org](http://www.ensembl.org)) with the longer

pGL2-L5A3 plasmid containing *ATXN2* upstream sequence including -5583 bp from the TSS. We observed that the average expression was reduced by 25 and 33% when the longer upstream sequence was included compared with the shorter one, in both HEK293 and SH-SY5Y cells, respectively (*t*-test 5A3 versus L5A3;  $P < 0.001$  in HEK293 and  $P < 0.01$  in SH-SY5Y; Fig. 4A). We then determined the expression of *ATXN2-luc* from 12 different pGL2-5A3 plasmids each with different deletions from the upstream end of the cloned *ATXN2* promoter fragment [promoter deletions 1–12 (PD1–PD12)]. For deletions PD1–PD11, increasing deletion of the upstream end of the *ATXN2* promoter was associated with increased *ATXN2-luc* expression in HEK293 and SH-SY5Y cells (Fig. 4B). Expression from the non-mutated pGL2-5A3 plasmid compared with that of any of PD1–PD11 was significantly different (*t*-test: 5A3 versus PD1,  $P < 0.001$ , HEK293 and SH-SY5Y; 5A3 versus PD2,  $P < 0.05$ , SH-SY5Y). The data suggested the existence of inhibitory promoter elements between -1062 and -816 and -55 and +41 that were progressively removed by increasing PD, whose regulatory proteins are expressed in both HEK293 and SH-SY5Y cells. The deletion of some regions resulted in no change in expression (between -816 and -493 in HEK293 cells and -1045 and -892 and -493 and -55 in SH-SY5Y cells), and one region resulted in significantly reduced expression when deleted (-555 and -493 in SH-SY5Y cells,  $P < 0.05$ ). For the final deletion PD12, *ATXN2-luc* average expression was reduced to 57 and 39% of that for the non-deleted pGL2-5A3 control in HEK293 and SH-SY5Y cells, respectively.

### ***ATXN2* interstitial PD and *ATXN2-luc* expression**

We determined the expression of *ATXN2-luc* from 16 different pGL2-5A3 plasmids each with different overlapping interstitial deletions in the *ATXN2* promoter of ~100 bp in length [interstitial PDs 1–16 (IPD1–IPD16)] and four smaller deletions (IPD20–IPD23; Fig. 4C). In HEK293 cells, all of the IPD1–IPD15 similarly reduced the average *ATXN2-luc* expression compared with the non-mutated 5A3 control plasmid in multiple independent experiments. We also observed similar expression among IPD1–IPD15 in SH-SY5Y cells except that unlike in HEK293 cells, the non-mutant 5A3 control plasmid expressed similar to constructs with IPD1–IPD15. The IPD16 and IPD20–IPD24 resulted in similar expression changes between HEK293 and SH-SY5Y where, in general, the IPD20–IPD22 resulted in no reduced (HEK293) or slightly elevated (SH-SY5Y) expression, and the IPD16 and IPD23 caused the lowest expression observed among all IPDs tested.

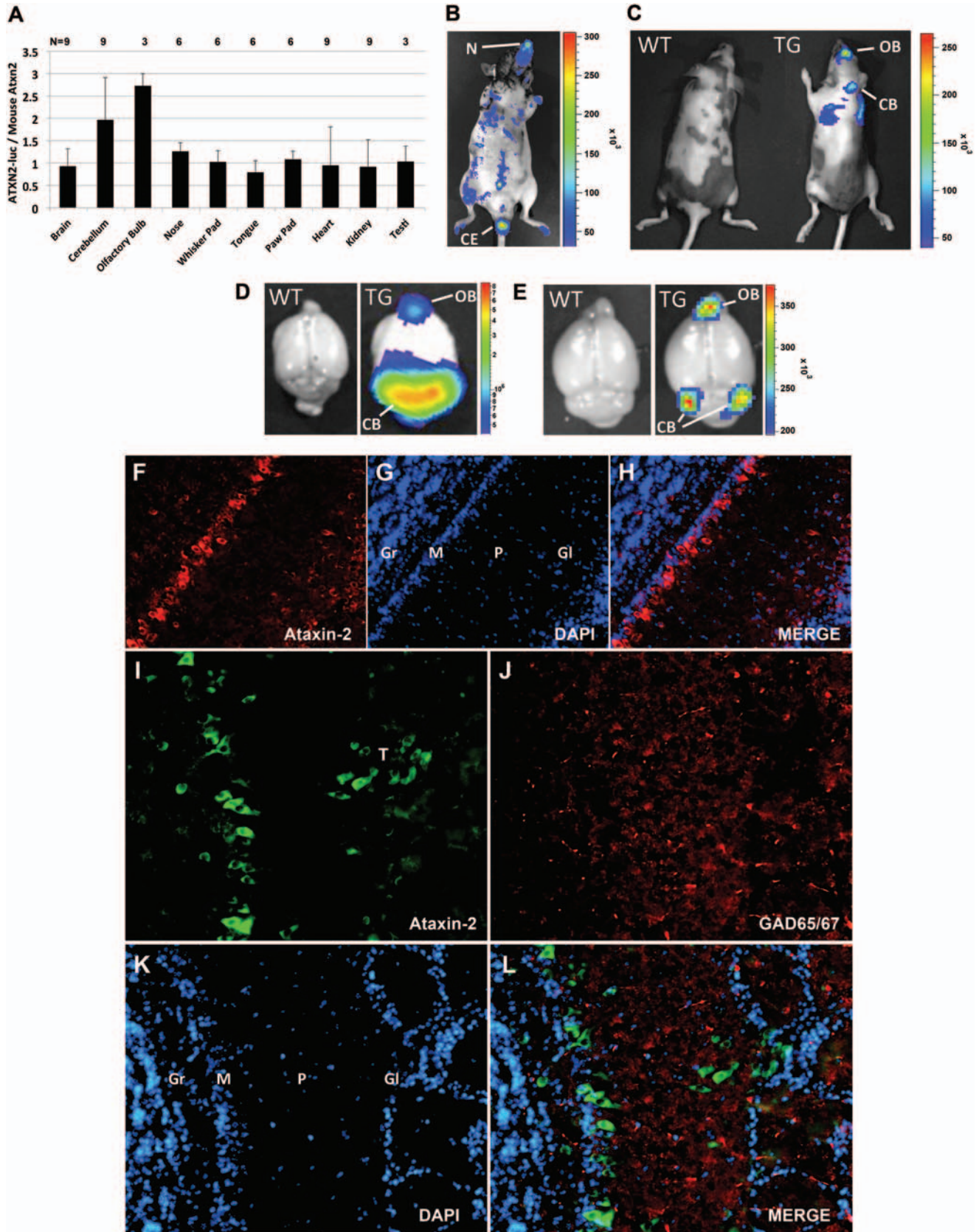
### **Luciferase assays of *ATXN2-luc* with the ETS1 site mutated or with ETS1 overexpressed demonstrated ETS1 supports *ATXN2* expression**

The similarly reduced *ATXN2-luc* expression observed when IPD16 or IPD23 were present (Fig. 4C) led us to closely evaluate the 23 bp region (+87 to +109) that is shared between these two deletions for TF-binding sites. TF prediction

software revealed a consensus sequence for ETS TF binding on the *ATXN2* negative strand between +96 and +103 of the *ATXN2* gene relative to the TSS. The ETS element sequence in *ATXN2* has 100% homology to the ETS element consensus sequence described in the majority of promoters, CCGGAAGT (28). We created two additional pGL2-5A3 construct modifications including a 14 bp deletion encompassing the ETS-binding site (including +94 to +107 sequence CGACTTCCGGTAAA in *ATXN2*) designated D14, and a 3 bp TCC→CGA mutation (+99 to +101 on the positive strand) in the core GGAA of the ETS element, designated mCGA, corresponding to GGA→TCG on the negative strand (Fig. 5A). The resulting mutated ETS element sequence of CCTCGAGT is predicted to have no affinity for binding by ETS TFs. The mCGA mutation resulted in 51 and 35% reduction in average *ATXN2-luc* expression compared with the non-mutated 5A3 control construct, while the D14 deletion reduced expression by 76 and 65% in HEK293 and SH-SY5Y cells, respectively (Fig. 5B). The expression of *ATXN2-luc* with either the mCGA or the D14 mutations were detectable by immunoblotting with anti-luciferase (Fig. 5C). We also made seven additional *ATXN2* promoter-luciferase constructs with 5 bp tandem deletions to confirm that the deletion of the ETS element reduced expression greater than any same-sized deletions in the region upstream and downstream of the ETS element. A 5 bp deletion including the ETS element GGAA core (Prl-D4) reduced expression the most (by 95%), while neighboring 5 bp deletions compromising the ends of the ETS element (Prl-D3 and Prl-D5) reduced expression by ~80%, and other deletions farther away from the ETS element had minimal effect (Fig. 5D). This demonstrated that the ETS element is required for *ATXN2* expression. To support this conclusion, we determined the effect of ETS1 overexpression on *ATXN2-luc* in luciferase assays. Overexpression of ETS1 resulted in a statistically significant 2.4-fold increase in *ATXN2-luc* expression in luciferase assays, but overexpression of ETS1 had no effect on inducing the expression of *ATXN2-luc* when the D14 deletion was included (Fig. 5E).

### **Electromobility supershift assays demonstrated that ETS1 bound an *ATXN2* probe including the ETS1-binding site**

We conducted electromobility shift assays (EMSA) with antibody supershift to test that the D14 region of the *ATXN2* gene interacted with the ETS1 TF and other ETS TFs. We utilized a 21 bp probe containing *ATXN2* sequence encompassing the D14 region. Supershifted bands were observed for ETS1 and ELF2 from SH-SY5Y nuclear lysate that were not shifted when antibodies to these TFs were excluded (Fig. 6A). Additional EMSAs are provided as Supplementary Material. These supplemental figures show the following: positive supershift for ETS1, ELF2 and GABP $\alpha$  but not for ELF1 or STAT3 (the latter used as a negative control) in both HEK293 and SH-SY5Y cell nuclear lysates (Supplementary Material, Fig. S2A and B); greater probe shift for the wild-type *ATXN2* probe versus mutant mCGA *ATXN2* probe and lack of shift bands when SH-SY5Y protein lysate was excluded (Supplementary Material, Fig. S2C).



### Chromatin immunoprecipitation PCR assays demonstrated endogenous ETS1 was bound to the native *ATXN2* promoter

To demonstrate that endogenous ETS1 interacted with the native *ATXN2* promoter, we conducted chromatin immunoprecipitation (ChIP) PCR analysis. ChIP PCR experiments using SH-SY5Y cell lysates demonstrated increased *ATXN2* amplicon abundance for ChIPs conducted with anti-ETS1 versus rabbit IgG control or no antibody control after two or three protein-A-agarose column washes, when either examined by agarose gel electrophoresis (Fig. 6B) or quantitatively by qPCR. qPCR demonstrated binding ratios of 7–30. The ChIP experiment was repeated three times using SH-SY5Y cells with the same result.

### Changes of ETS1 expression affect endogenous ataxin-2 abundance

To demonstrate that ETS1 regulates *ATXN2* expression, we overexpressed full-length ETS1, a dominant negative (dn)-ETS1 fragment or an ETS1 short-hairpin RNA (shRNA) and assessed ataxin-2 abundance by western blotting. Overexpression of ETS1 resulted in significant increases in ataxin-2 abundance in both HEK293 and SH-SY5Y cells (Fig. 6C and D), while that of dn ETS1 resulted in a significant reduction in ataxin-2 expression in these cell lines (Fig. 6E and F). Additionally, the overexpression of an shRNA plasmid targeting the expression of ETS1 resulted in significantly lower ataxin-2 expression, while an shRNA plasmid against green fluorescent protein (GFP) had no effect (Fig. 6G). IF labeling demonstrated that ETS1 overexpression increased endogenous ataxin-2 expression and localization. We observed a subset of cells overexpressing ETS1 with increased endogenous ataxin-2 expression with ataxin-2 often localizing to a perinuclear region or forming aggregate bodies (Fig. 6H–K). IF labeling also increased ataxin-2 abundance in nearly all SH-SY5Y cells overexpressing ETS1 (Fig. 6L). Note that, we were unable to demonstrate an effect of mutant *ATXN2* CAG repeats on ETS1 ability to transactivate *ATXN2* (not shown).

## DISCUSSION

A promising approach for developing therapies for polyQ disorders is to lower the disease gene expression. The rationale for this is that mutations in polyQ diseases primarily result in a gains of normal or toxic functions, although there can

also be partial functional losses (29). Other therapeutic modalities for polyQ diseases are problematic due to lack of knowledge on gene functions that are specifically related to disease onset or progression. To support our efforts to develop therapeutics for SCA2, we have rigorously characterized the control of *ATXN2* expression, including validation of our study construct *in vivo*. We identified features of *ATXN2* expression control that might be exploited therapeutically and developed hypotheses on how CAG length controls expression with relevance to other polyQ diseases.

We discovered evidence for negative regulatory elements distributed throughout the *ATXN2* gene upstream region that may support expression control and tissue-specific expression. Promoter-luciferase assay studies showed that *ATXN2-luc* constructs with longer upstream sequences generally had lower *ATXN2-luc* expression than those with shorter upstream sequences. This is likely due to the presence of multiple inhibitory elements throughout the *ATXN2* promoter. This conclusion is consistent with observations made by Aguiar *et al.* (2,26) who showed that an *ATXN2-luc* construct possessing *ATXN2* upstream sequence –436 to +362 expressed  $1.6 \pm 0.1$  times higher than one possessing a longer *ATXN2* upstream sequence of –2912 to +362 (mean and SD for F9 cells and SH-SY5Y cells). These findings suggest the existence of inhibitory elements distributed throughout the *ATXN2* promoter that may be critical for fine-tuning expression in a developmental or tissue-specific manner.

We created *ATXN2-luc* transgenic mice to verify that the region of the *ATXN2* promoter and 3'-UTR in our study replicated expression similar to the endogenous *Atxn2* gene. Queries of the Allen Brain Atlas (Allen Institute for Brain Science) (30,31) showed that *Atxn2* is highly expressed in Purkinje cells, hippocampus (CA1–3 and dentate gyrus) and the mitral layer of the OB compared with other mouse brain tissues. Analysis of *ATXN2-luc* expression in *ATXN2-luc* transgenic mice by qPCR and IVIS imaging demonstrated consistencies with the Allen Brain Atlas *in situ* hybridization data. For most tissues, *ATXN2-luc* expression was 1:1 versus endogenous *Atxn2* by qPCR, and *ATXN2-luc* was elevated in the cerebellum for a subset of mice and in the OB, but on average *ATXN2-luc* in the cerebellum was not statistically different from 1:1 versus *Atxn2*. We next performed immunohistochemical (IHC) staining of the OB sections from wild-type mice to confirm the Allen Brain Atlas data, showing that *ATXN2* is expressed high in mitral cells, and to support biological relevance for *ATXN2-luc* expression in the OB. IHC confirmed highest expression of ataxin-2 in mitral cells and

**Figure 3.** *ATXN2-luc* expression *in vivo* was elevated in the cerebellum and OB compared with endogenous *ATXN2*. (A) For most tissues, the average expression of *ATXN2-luc* to endogenous mouse *Atxn2* was 1:1 by qPCR. *ATXN2-luc* expression was high in some mice in the cerebellum and OB relative to mouse *Atxn2* but the average ratio in the cerebellum was not significantly different from that for other tissues. qPCRs were run in triplicate and the reported values represent the means among mice  $\pm$  SD. (B–E) Evaluation of *ATXN2-luc* expression on the IVIS. (B) *ATXN2-luc* expression in the nose (N) and cauda epithelium (CE) of a *ATXN2-luc* transgenic mouse. (C) Detection of *ATXN2-luc* in the OB and cerebellum (CB) in a 7-month-old *ATXN2-luc* transgenic mouse (TG) and lack of signal in a wild-type littermate (WT). (D) *ATXN2-luc* detected in the OB and CB of a 2-month-old *ATXN2-luc* transgenic mouse and lack of signal in a wild-type littermate. (E) *ATXN2-luc* detected in the OB and CB of a 7-month-old *ATXN2-luc* transgenic mouse and lack of signal in a wild-type littermate. (F–L) IF detection of endogenous *Atxn2* in the OB of wild-type C57Bl/6 mice. (F) Ataxin-2 detected with ataxin-2 mAb in mitral cells and tufted cells in the glomerular layer ( $\times 10$  magnification). (G) Same section as (F) stained with DAPI. (H) Merge of (F) and (G). (I) Ataxin-2 detected with polyclonal antibody 1080 in mitral cells and tufted cells in the glomerular layer ( $\times 20$  magnification). (J) Same section as (I) stained with anti-GAD65/67. (K) Same section as (I) stained with DAPI. (L) Merge of (I)–(K). Note that no ataxin-2 was detected in GAD65/67-positive interneurons. Labels: T, tufted cells; Gr, granule layer; M, mitral layer; P, external plexiform layer; Gl, glomerular layer. Bars = 100  $\mu$ m.

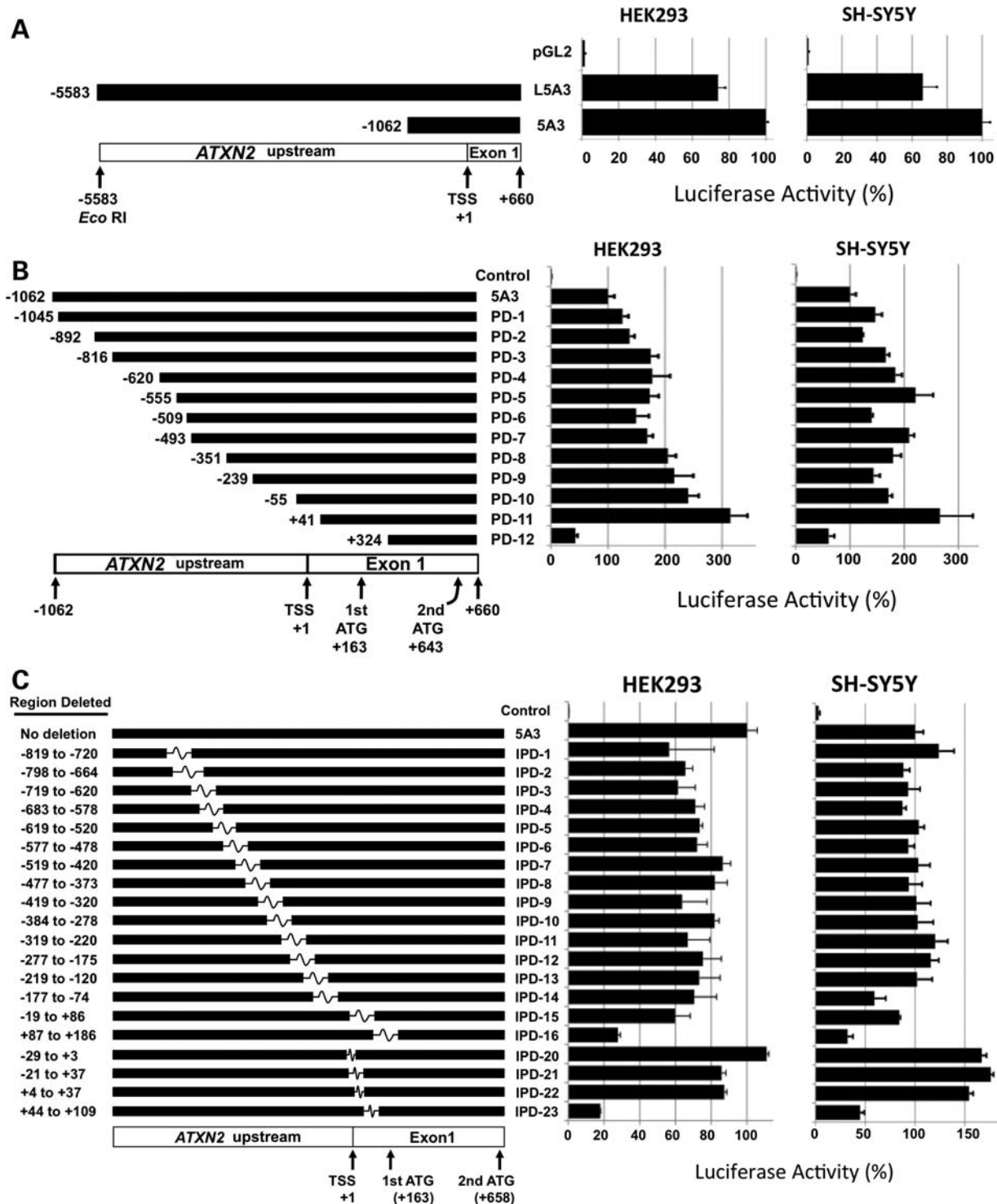


**Figure 4.** Effects of *ATXN2* PDs on *ATXN2-luc* expression and identification of an *ATXN2* 5'-UTR region (+87 to +109) accounting for the majority of *ATXN2* expression. (A and B) Effect of increasing *ATXN2* PD on *ATXN2-luc* expression. (A) The long *ATXN2* upstream sequence contained in plasmid pGL2-L5A3 reduced *ATXN2-luc* expression similarly in HEK293 and SH-SY5Y cells compared with the shorter upstream sequence in pGL2-5A3. (B) Further decreases in the *ATXN2* promoter length in pGL2-5A3 correlated with increases in *ATXN2-luc* expression. A plateau where no successive increased expression was observed between -816 and -351 in HEK293 cells and -555 and -55 in SH-SY5Y cells. PD12 spans the smaller +87 to +109 5'-UTR region and resulted in expression reduction in both cell lines. (C) Effect of *ATXN2* IPDs in pGL2-5A3 on *ATXN2-luc* expression. Only deletions IPD16 and IPD23 including the +87 to +109 5'-UTR region caused reduced expression in both HEK293 and SH-SY5Y cells compared with the pGL2-5A3 plasmid that contains no interstitial deletion. For each of (A)–(C), a graphic representation is provided (left) where the upstream/promoter sequence present is represented by a black bar and for (C) where the sequence that has been interstitially deleted is represented by a white box. Relative expression in HEK293 and SH-SY5Y cells for each deletion (right), controlled with *SV40-Renilla* luciferase. Nucleotides are numbered such that +1 corresponds to the transcriptional start site or first base in the 5'-UTR. Values are mean  $\pm$  SD from three independent transfections each read in triplicate.

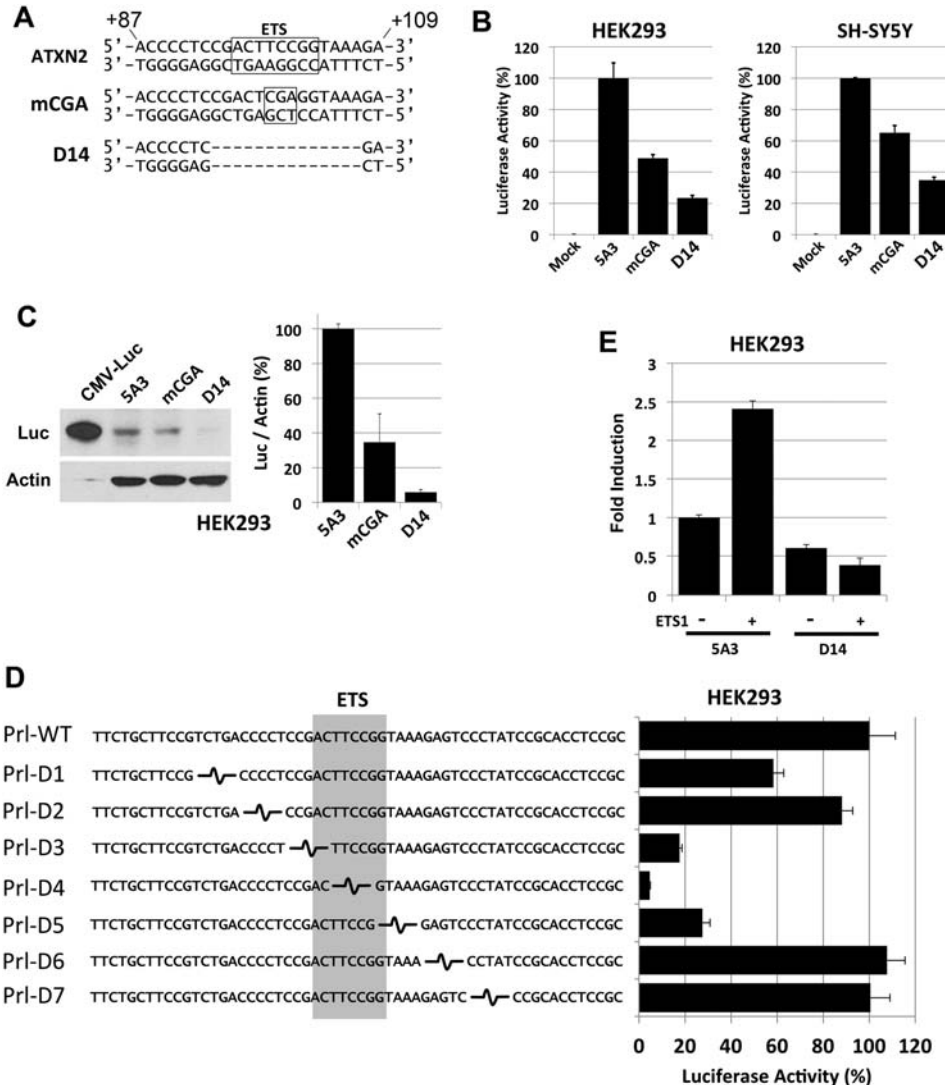


**Figure 5.** A 14 bp region within the +87 to +109 *ATXN2* 5'-UTR region contains an ETS TF-binding site and accounts for the majority of *ATXN2* expression. (A) Both strands of the *ATXN2* sequence from +87 to +109 are shown and the position of an ETS TF-binding site oriented from +103 to +96 on the *ATXN2* minus strand is indicated (box). mCGA represents a TCC → CGA mutation with the ETS TF-binding site made in the *ATXN2-luc* expression plasmid pGL2-5A3. This mutation alters the ETS TF consensus sequence core on the *ATXN2* minus strand from GGAA → TCGA to abrogate binding by ETS TFs. D14 represents a 14 bp deletion spanning the ETS TF-binding site in pGL2-5A3. (B) Luciferase assays comparing no mutation to the mCGA and D14 mutations in HEK293 and SH-SY5Y cells. The mCGA mutation resulted in 51 and 35% reduction in the average *ATXN2-luc* expression in HEK293 and SH-SY5Y cells, respectively, relative to no mutation. The D14 mutation resulted in 76 and 65% reduction in the average *ATXN2-luc* expression in HEK293 and SH-SY5Y cells, respectively, relative to no mutation. Values are means and SD from three independent transfections each read in triplicate and expression was controlled with *SV40-Renilla* luciferase. (C) Western blot showing that the mCGA and D14 mutations in pGL2-5A3 reduced *ATXN2-luc* expression in HEK293 cells compared with no mutation. The D14 mutation reduced *ATXN2-luc* to background. (D) Effect of seven tandem 5 bp deletions in the *ATXN2* promoter on *ATXN2-luc* expression. Deletions were made by ligating annealed oligonucleotides spanning 58 bp of the *ATXN2* promoter into a rat prolactin-luc minimal promoter construct. Deletions overlapping the ETS element reduced expression while those flanking the ETS element had no effect or minimal effect. (E) ETS1 activation of *ATXN2* depends on the ETS-binding site. Overexpression of ETS1 increased *ATXN2-luc*. Inclusion of the D14 deletion in *ATXN2-luc* blocked the ability for ETS1 to increase *ATXN2-luc* expression. Values are means and SD from three independent transfections each read in triplicate and expression was controlled with *TK-Renilla* luciferase.

equally high expression in tufted cells. Collectively, these data suggest that *ATXN2-luc* in transgenic mice is expressed much like endogenous mouse *ATXN2*, with the caveat that differences in cerebellar *ATXN2-luc* expression among mice might reflect reduced stability of expression control when the promoter is truncated. IVIS imaging also identified *ATXN2* expression outside the central nervous system including high expression in the nose and cauda epididymis. Previously,

*ATXN2* knockout mice were characterized as having reduced fertility (32) that may relate to loss of *ATXN2* expression in developing and mature sperm of the cauda epididymis.

Strong expression of *ATXN2* in the OB and nose are interesting in light of marked obesity in *ATXN2* knockout mice (25,32). In unpublished experiments, we have now shown that obesity is the cause of severe hyperphagia that is even present in heterozygote animals. It is possible that changes

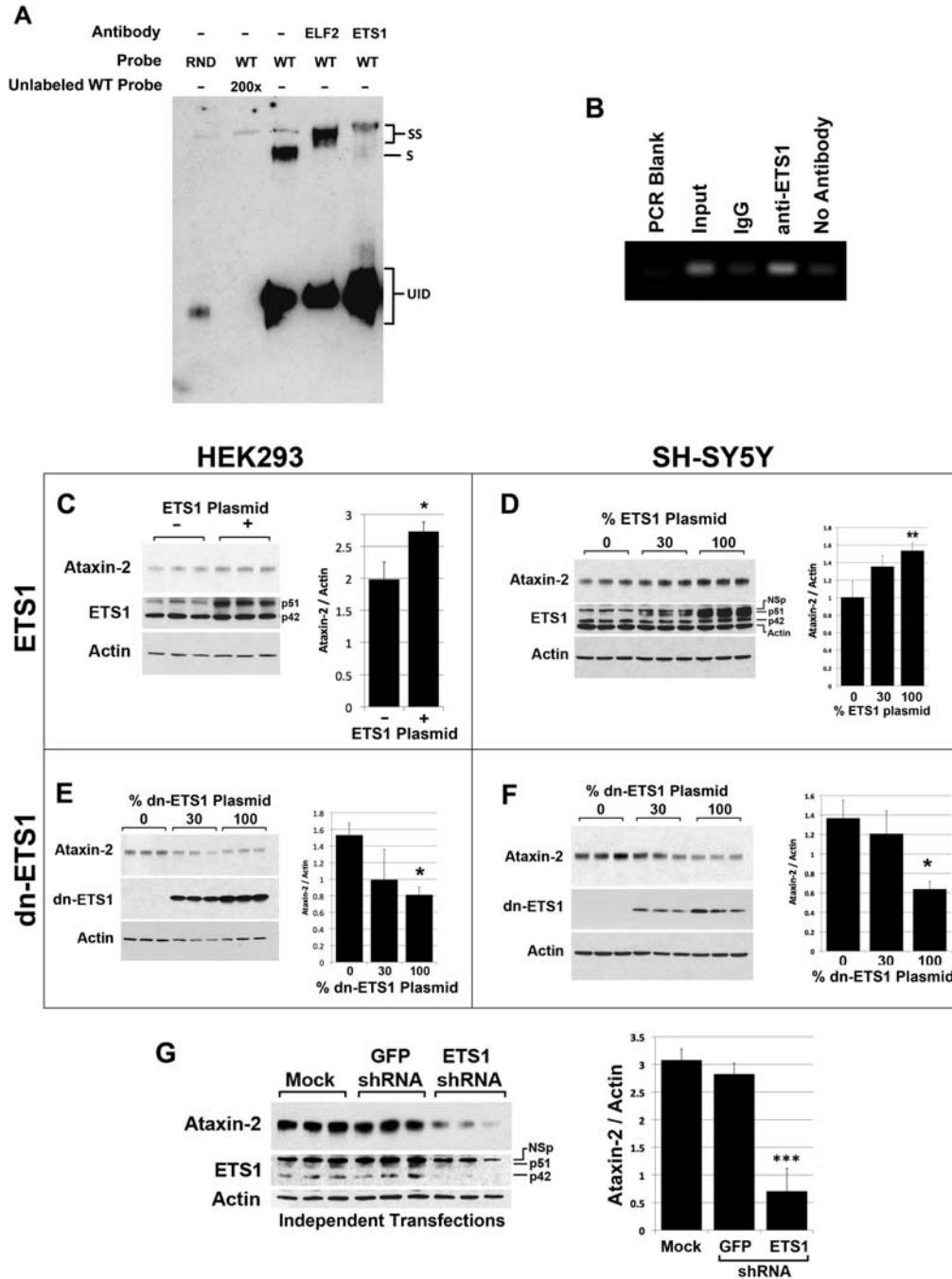


**Figure 6.** ETS1 interacts with the ETS1 site in *ATXN2* and regulates *ATXN2* expression. (A) EMSA verified ETS1 binds a probe containing the ETS1 as well as ELF2 in SH-SY5Y nuclear lysate included as a positive control. EMSA supershift assays using HEK293 and SH-SY5Y nuclear lysates with various electrophoresis times and additional controls (including ELF2) are shown in Supplementary Material, Fig. S2. (B) ChIP PCR analysis evaluated by agarose gel electrophoresis demonstrated endogenous ETS1 in SH-SY5Y cells bound the ETS1 site in *ATXN2*, as indicated by pull-down of the complex with anti-ETS1 but not rabbit IgG. When evaluated by qPCR binding ratios ranged from 7 to 30. Western blots showing that the overexpression of the 51 kDa isoform of ETS1 in HEK293 (C) and SH-SY5Y cells (D) increased Ataxin-2 expression. A non-specific band (NSp) was sometimes observed. Experiments were loaded in triplicate. Western blots showing that the overexpression of dn ETS1 in HEK293 (E) and SH-SY5Y cells (F) reduced Ataxin-2 expression. Experiments were loaded in triplicate. (G) Western blot showing that the underexpression of *ETS1* by transfection of an *ETS1* shRNA resulted in reduced Ataxin-2 expression in SH-SY5Y cells. No change for Ataxin-2 or ETS1 expression was observed when a control GFP shRNA was used. Each lane represents an independent transfection. Significance was determined by ANOVA Bonferroni post-tests; \* $P < 0.05$ , \*\* $P < 0.01$  and \*\*\* $P < 0.001$ . Effect of ETS1 overexpression on endogenous ataxin-2 expression in HEK293 cells (H–K) and SH-SY5Y cells (L) determined by IF labeling: cells overexpressing the 51 kDa isoform of ETS1 had increased ataxin-2 expression localized to a perinuclear space (H). Some cells overexpressing ETS1 showed diffusely distributed ataxin-2 expression (I) or aggregations of ataxin-2 (J). HEK293 cells not transfected with ETS1 showed low and diffuse expression of both ETS1 and ataxin-2 (K).  $\times 30$  magnification; bar, 100  $\mu\text{m}$ ; equal exposure settings were used. (L) Nearly all ETS1-transfected SH-SY5Y cells overexpressing ETS1 had detectable ataxin-2 expression. DAPI was used to identify untransfected cells.  $\times 20$  magnification; bar, 100  $\mu\text{m}$ .

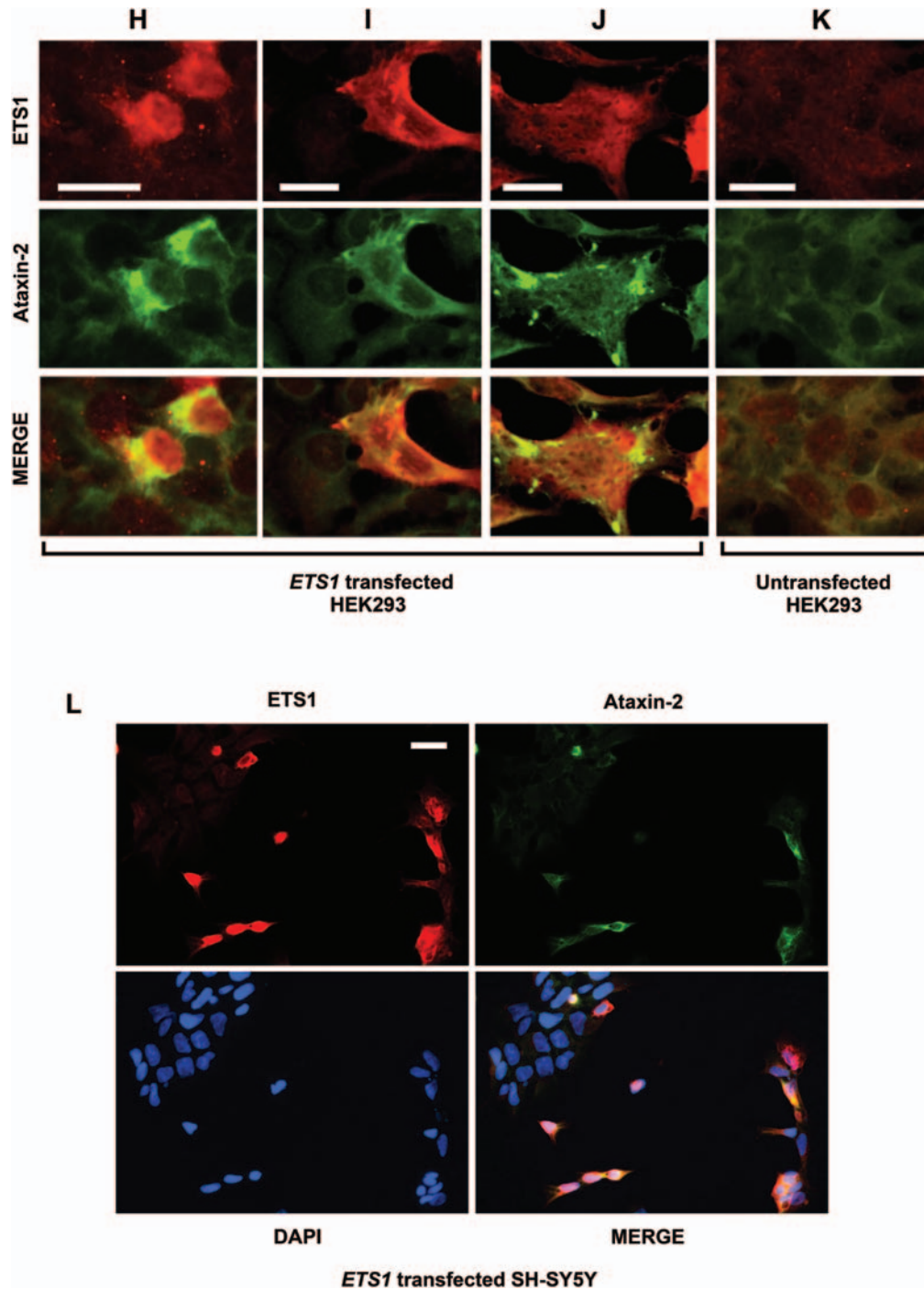


Figure 6. Continued.

in olfaction caused by *ATXN2* loss in mitral cells of the OB and other cells involved in olfaction may decrease reward signals mediated by smell. This hypothesis is supported by a central role of *dAtx2* in olfactory habituation in the fly (33) and the finding of impaired olfaction in SCA2 patients (34).

The impact of CAG repeat expansion on gene expression and protein abundance is not completely understood for other polyQ disease genes. For *ATXN2*, features that might affect expression include (i) the location of the *ATXN2* CAG

repeat within a CpG island in exon 1 (26,35) raising the possibility that CAG expansion can influence transcription by altering the proximity of TFs acting on either side of the repeat and (ii) the close proximity of the CAG repeat to the start codon potentially influencing *ATXN2* translation. The increase in the CAG repeat length from 1 CAG to 22 CAGs increased the expression of ataxin-2-luciferase 4-fold. We speculate that this may be due to increased protein stability or facilitation of non-ATG initiated translation as was

observed for SCA8 (36). The longest CAG repeats in both *ATXN2* and *ATXN2-luc* caused reduced protein abundance when evaluated by luciferase assays or western blotting, but we could find no evidence for long CAG repeats influencing transcription by qPCR. This observation may reflect reduced solubility for the polyQ-expanded ataxin-2 and ataxin-2-luc proteins or may be due to other factors related to the RNA including abnormal translation, pre-mRNA processing caused by thermodynamically stable CAG hairpinning (37) or RNA aggregation as for *DMPK* (38). Translational regulation by the *ATXN2* CAG repeat might be facilitated by its close proximity to the start codon (separated by only four codons) and could be regulated by RNA-binding proteins interacting with the CAG repeat hairpin (39). Both *ATXN7* and *HTT* have CAG repeats near their start codons, at codons 30 and 18, respectively, and we hypothesize that CAG repeat expansion might also regulate the translation of these genes. Our study of CAG repeat length on *ATXN2* expression raises new hypotheses that will require evaluation in future work.

Analysis of the *ATXN2* promoter revealed the presence of an ETS element in the *ATXN2* 5'-UTR identified by detailed deletion analysis. We also noted that none of the predicted sites for ZBRK1 binding localized to this region nor did we identify any other *ATXN2* promoter regions that reduced *ATXN2* expression upon deletion. As seven ZBRK1 sites were predicted in the *ATXN2* promoter (27), our data support that PDs including single ZBRK1 sites are not sufficient to reduce *ATXN2* expression. However, our finding is consistent with Aguiar *et al.* (26) who evaluated two *ATXN2-luc* constructs lacking the ETS element (−30 and downstream, plasmids C2 and C6 in their study) that had expression close to negative controls. Because the ETS element was 59 bp upstream of the first of two in-frame ATGs that was also within some inhibitory deletions that we made, we mutated the ATGs individually to determine which were functional. Elimination of the upstream ATG had no effect on expression, while that of the downstream ATG reduced expression to a level similar to control assays. This indicated that *ATXN2* deletions containing both the ETS element and the first ATG reduced *ATXN2-luc* expression due to loss of the ETS element and that the second ATG was the functional start codon. This ETS element has 100% match to the consensus sequence for binding by ETS family TFs ETS1, ELF1 and GABP $\alpha$ , defined as CCGGAAGT (28). We demonstrated that ETS1, ELF2 and GABP $\alpha$  interacted with the ETS element by EMSA. Because we could not confirm that the overexpression of ELF1, ELF2 or GABP $\alpha$  could increase *ATXN2* expression, we limited ChIP and shRNA validations to the study of ETS1 only. ETS1 is expressed in mouse Purkinje cells higher than in any other cell type in the cerebellum, according to the Allen Brain Atlas (30) (Supplementary Material, Fig. S3) and a study describing ETS1 in developing brain (40). Roles for ETS TFs in ataxias are also supported by the observation that ataxin-1 transcriptionally activates *ETV5* (29).

In summary, we verified that the second in-frame ATG in *ATXN2* located five codons upstream from the CAG repeat is the functional start codon, resulting in a full-length ataxin-2[Q22] protein of 1152 amino acids, 160 amino acids shorter than assumed previously. We evaluated *ATXN2-luc* expression in transgenic mice and demonstrated high luciferase

expression in the mouse cerebellum, as expected, and high expression in the OB. IHC staining of the mouse OB revealed endogenous *ATXN2* expression in mitral cells. We speculate that loss of *ATXN2* expression in OB mitral cells in *ATXN2* knockout mice may account for obesity due to hyperphagia that we previously observed in these mice. Expression of *ATXN2-luc* in transgenic mice resembled endogenous *ATXN2* supporting that the length of the promoter studied in transgenic mice was sufficient to reflect the true pattern of *Atxn2* expression and the potential for using *ATXN2-luc* mice in the validation of experimental SCA2 therapeutics targeting *ATXN2* expression. We demonstrated that an ETS element in *ATXN2* is required for *ATXN2* expression. Ataxin-2 expression was increased in cells overexpressing ETS1, supporting that ETS1 regulates *ATXN2* expression. More work will be required to determine whether other TFs bind this region of the *ATXN2* promoter and whether they represent therapeutic targets for SCA2. As the deletion of the ETS element resulted in a major reduction *ATXN2* expression, this region may represent an opportune target for decoy oligonucleotide-based therapeutics (41–43).

## MATERIALS AND METHODS

### Cloning of pGL2-5A3

The preparation of plasmid pGL2-5A3 was a six-step cloning process beginning with our original *ATXN2* promoter plasmid pGL2-5. All amplifications for cloning in the study were made using the Expand High FidelityPLUS PCR System (Qiagen) and all clones that were created were verified by sequencing.

To clone plasmid pGL2-5, we amplified ( $T_A = 58^\circ\text{C}$ ) a 1431 bp fragment from genomic DNA including *ATXN2* upstream-5'-UTR sequence with forward primers ATX2A (5'-GCTAGATTAATTTTTAAAGGGTTTTGCAATG-3') and ATX2B (5'-TAGCACGCGTAAGAGCTCTG-3'). This fragment was digested with *AseI*, treated with T4 polymerase to fill the sticky end, redigested with *SacI*, then ligated to pGL2.Enhancer between the *SmaI* and *SacI* sites of the multiple cloning site (MCS). We next created plasmid pGL2a-5 by ligating a linker fragment made by annealing a 48mer (5'-TAAAGGCCAAGAAGGGCGGAAAGTCCAAATTGTA AACCGGTACTGTAG-3') to a 51mer (5'-TCGACTACAG TACCGGTTTACAATTTGGACTTTCCGCCCTTCTTGGC CTTT-3') between the *EcoNI* and *SalI* sites of pGL2-5. This linker eliminated the vector polyA and incorporated an *AgeI* site immediately downstream of the vector *luc* gene stop codon for use in later cloning of the 3'-UTR. In order to remove the sequence downstream of the pGL2 MCS *XhoI* site, we amplified ( $T_A = 55^\circ\text{C}$ ) the *luc* gene from pGL2 with primers LucXhoIA (5'-GCATCTCGAGATGGAAGACGC CAAAACATA-3') and LucAgeIB (5'-GCATACCGGTTT ACAATTTGGACTTTCCGCCCTTCT-3') and ligated this fragment in place of the original *luc* gene of pGL2a-5 between *XhoI* and *AgeI*. We named this clone as pGL2b-5. We then prepared plasmid pGL2b-5-3 by inserting a 1019 bp fragment of *ATXN2* 3'-UTR and downstream sequence amplified ( $T_A = 53^\circ\text{C}$ ) with primers *AgeIA* (5'-CGCTAACCGGTGTTGTAAGGCTGCCCTGGAGGA-3') and *SalIB* (*AtxnB2*) (5'-GCTAGTCGACAGCCTTCATGCCC

TCTGGATTT-3') into pGL2b-5 between the linker *AgeI* and the vector *SalI* site. Because pGL2b-5-3 contained the first *ATXN2* start codon but not the second in-frame start codon that we also wanted to study, we next added an additional exon 1 fragment including the second start codon and sequence up to and including the first CAG of the CAG repeat. This fragment was amplified ( $T_A=69^\circ\text{C} + 5\%$  dimethyl sulfoxide) from genomic DNA with primers *SacIv2A* (5'-CTCGCCGCTTCGC CGCAGCCAGGT-3') and *XhoIB* (5'-GAATGCCCTCGAGAG CCGTGGCCGAGGACGAGGAGAC-3'). This step also removed the vector sequence upstream of the *XhoI* site which in this plasmid immediately follows the first CAG of the CAG repeat. The resultant plasmid was named pGL2b-5A3. We then changed the start codon of the luciferase gene to CTG (leucine). This was accomplished by amplifying ( $T_A=55^\circ\text{C}$ ) the *luc* gene from pGL2 with primers *LucXhoIA2* (5'-GCATCTCGAGCTGGAAGACGCCAAAACATA-3') and *LucAgeIB* (see above) and ligating it in place of the *luc* gene of pGL2b-5A3 between *XhoI* and *AgeI*. We named the final clone as pGL2-5A3.

### Lengthening the *ATXN2* promoter in pGL2-5A3 to create pGL2-L5A3

We lengthened the *ATXN2* promoter in pGL2-5A3 by replacing an *ATXN2* promoter fragment excised from pGL2-5A3 with a longer fragment obtained from a bacterial artificial chromosome (BAC) clone RP11-798L15 (Empire Genomics). A 5656 bp *ATXN2* upstream sequence fragment was excised from the BAC plasmid with *EcoRI* and *NotI* and ligated into plasmid pCR4-TOPO. The fragment was then excised with *PmeI* (in the MCS of pCR4-TOPO) and *NotI* (in *ATXN2*) and ligated into pGL2-5A3 prepared with *HpaI* and *NotI*. The resulting plasmid included *ATXN2* upstream sequence starting at position -5502 from the TSS and was named pGL2-L5A3.

### Mutating *ATXN2* start codons in pGL2-5A3

Mutation of the second *ATXN2* start codon was accomplished by preparing annealed linkers that were then ligated into their corresponding locations in the *ATXN2* exon 1 portion of pGL2-5A3, replacing the wild-type start codon. To change the first ATG to CTG, we prepared a 137 bp double-stranded linker by annealing the two oligonucleotides *ATG2\_sense* (5'-CCTCACCCcTGTCGCTGAAGCCCCAGC-3') and *ATG1\_antisense* (5'-TCGAGCTGGGGCTTCAGCGACAgGGTGAG GGGCC-3'). Annealing these oligonucleotides created *ApaI* and *XhoI* sticky ends ready to ligate into pGL2.5A3 between the same two restriction sites. To mutate the first ATG to CTG in pGL2-5A3, we utilized a custom mutagenesis service (GenScript). Plasmids were verified by sequencing and were named pGL2.5A3(mATG1) and pGL2.5A3 (mATG2).

### Cloning upstream deletions of pGL2-5A3

Deletions of the upstream end of the *ATXN2* sequence were accomplished by timed exonuclease III digestion. We first modified pGL2-5A3 by the insertion of an oligonucleotide linker upstream of the sequence to be deleted introducing

two new restriction sites including *NsiI* on the upstream side, producing an exonuclease III resistant 3' overhang, and *SpeI* on the downstream side, producing an exonuclease III susceptible 5' overhang. The linker was made by annealing the two oligonucleotides *EAB-A* (5'-GATCATGCATCTC GAGACTAGTAGCT-3') and *EAB-B* (5'-AGCTACTAGTC TCGAGATGCATGATC-3'). The linker was then ligated into the *HpaI* restriction site located just the upstream of the *ATXN2* upstream sequence insert in pGL2-5A3. We performed timed exonuclease III digestions of *NsiI* and *SpeI* double-digested plasmid using the Erase-A-Base (Promega) kit following the vendor's protocol. Twenty-five different deletions in pGL2-5A3 were verified by sequencing, of which 12 were used in the study, designated PD1–PD12.

### Cloning of IPDs in pGL2-5A3

IPDs were made by two methods. IPD1–IPD19 were made by a two-step PCR method where each deletion was ~100 bp in length. In the first step for any particular deletion, two PCRs were conducted. In one reaction, the reverse primer consisted of a ~30 bp hybrid primer made of ~15 bp sequence located on either side of the 100 bp region to be deleted and a forward primer across a unique restriction site for cloning (either *HpaI* or *BamHI*). In the other reaction, the forward primer consisted of a ~30 bp hybrid primer also made of the ~15 bp sequence located on either side of the 100 bp region to be deleted and a reverse primer across a unique restriction site for cloning (either *BamHI* or *XhoI*). These two reactions resulted in two amplicons with 15 bp shared sequence that would prime one another in the PCR performed in the second step, each with unique restriction sites on their extreme ends for cloning. To perform the second step, we first gel purified the amplicons from the first step using the Qiaex II Gel Extraction Kit (Qiagen) and then used 1  $\mu\text{l}$  (2 ng) of each in the second-step PCR including the two primers that prime at the unique restriction sites that were also used in the first-step PCRs. This second step resulted in a single amplicon containing the 100 bp deletion with unique restriction sites for cloning on each end. The amplicon from the second step was double-digested (with either *HpaI* and *BamHI*, *BamHI* and *XhoI* or *HpaI* and *XhoI*), gel purified using Qiaex II and ligated into pGL2-5A3 prepared with the same two enzymes. Deletions were verified by sequencing. The primers used to prepare each IPD clone of pGL2-5A3 are provided in Supplementary Material, Table S1, and the combinations how they were used in step 1 PCRs are in Supplementary Material, Table S2.

The remaining IPD clones (IPD20–IPD31) were made by annealing oligonucleotide pairs designed to create short *ATXN2* promoter fragments containing the desired deletions flanked by cohesive ends ready to ligate to pGL2-5A3 prepared by double-restriction digestion (either *BamHI* and *PmlI*, *PmlI* and *NotI*, *NotI* and *SacI* or *SacI* and *ApaI*). The oligonucleotides and the corresponding combination of restriction enzymes used to create each of these IPDs are provided in Supplementary Material, Table S3.

### Cloning of IPDs in pPrl-luc

We cloned a short fragment of the *ATXN2* 5'-UTR into pPrl-luc, a plasmid expressing luciferase from a rat minimal

prolactin promoter. The *ATXN2* fragment was 58 bp long with the ETS1-binding site at its center. The fragment corresponded to *ATXN2* +72 to +129 bp. Inserts were prepared by annealing sense and antisense oligonucleotides with or without deletions (Supplementary Material, Table S4). Annealing created a *SacI* site upstream and a *BglIII* site downstream. Inserts were ligated into pPr1-luc between the *SacI* and *BglIII* sites located between the prolactin minimal promoter and the luciferase.

### Addition of CAG tracts into pGL2-5A3

We modified pGL2-5A3 by addition of different CAG tracts including 108 bp of *ATXN2* exon 1 sequence downstream of the CAGs. Because pGL2-5A3 has a CAG1 tract but excludes the 108 bp exon 1 sequence downstream, we first made plasmid pGL2-5Aa3, identical to pGL2-5A3, but including the extra 108 bp exon 1 sequence. pGL2-5Aa3 was created by first preparing an insert made by annealing oligoCAG1-sense (5'-CCTCACCATGTGCTGAAGCCCCAGCCGCCG CCCGCGGCTGCCAATGTCCGCAAGCCCCGCGGCAGC GGCCTTCTAGCGTCGCCCGCCGCCGCGCCTTCGCCG TCCTCGTCCTCGGTCTCCTCGTCCTCGGCC-3') with oligoCAG1antisense (5'-TCGAGGGCCGAGGACGAGGA GACCGAGGACGAGGACGGCGAAGGCGCGGCGGCGG GCGACGCTAGAAGGCCGCTGCCGCCGGGCTTGCGGAC ATTGGCAGCCGCGGGCGGCGGCTGGGGCTTCAGCGAC ATGGTGAGGGGCC-3'). Annealing these oligonucleotides created *ApaI* blunt and *XhoI* sticky ends ready to ligate into pGL2.5A3 between the same two restriction sites. In order to create longer CAG tracts, we used a PCR approach: Using primers *SacI*-AA (5'-GGCAGAGCTCGCCTCCCTCCGC CTCAGAC-3') and *XhoI*-BB (5'-GCATCTCGAGGGCCGA GGACGAGGAGAC-3'), we amplified *ATXN2* exon 1 fragments including CAG tracts of lengths 22, 58 and 102 CAGs. Template plasmids are described in Ng *et al.* (44). These inserts were ligated into pGL2-5A3 prepared by *SacI* and *XhoI* digestion. The resultant plasmids were named pGL2-5B3, pGL2-5C3 and pGL2-5D3 (containing 22, 58 and 102 CAGs, respectively) and were sequenced to verify the CAG number. The CAG tract in pGL2-5B3 was the common normal length allelic form (CAG)<sub>8</sub>CAA(CAG)<sub>4</sub>CAA(CAG)<sub>8</sub>, while the CAG tracts in pGL2-5C3 and pGL2-5D3 did not include CAA interruptions.

### Addition of TK-Renilla cassettes into pGL2-5Aa3, pGL2-5B3, pGL2-5C3 and pGL2-5D3

We modified the plasmids pGL2-5Aa3, pGL2-5B3, pGL2-5C3 and pGL2-5D3 by the addition of a fragment containing TK-Renilla luciferase. We amplified the TK-Renilla-polyA insert from the plasmid pRL-TK (Promega) with primers TKRenSalA (5'-CTGGCGTCGACGATCTAAATGAGTC TTC-3') and TKRenSalB (5'-CAAGGTCGACGCCACCT GGATCCTTATC-3'), prepared the insert by *Sall* digestion and ligated it into the *Sall* site in each of the target plasmids. Sequencing confirmed the selection of plasmids with TK-Renilla oriented in the opposite direction compared with *ATXN2-luc*. The resultant plasmids were named pGL2-5Aa3-TK-rLuc, pGL2-5B3-TK-rLuc, pGL2-5C3-TK-rLuc and

pGL2-5D3-TK-rLuc. These plasmids were used in the qPCR experiment shown in Fig. 2C.

### Full-length *ATXN2* expression plasmids

We first acquired a 4 kb *ATXN2* upstream sequence (US) by PCR from human BAC clone RP11-798L15 using primers *HindIII*-Fwd (5'-TATAAAGCTTAAGCCTTCTGAAGTCC-3') and *NotI*-Rev (5'-GCTGCGGCCGCTGAGCGCATCGGAGGGCG-3'). The insert was ligated between the *HindIII* and *NotI* sites of the plasmid pAdTrack, also containing a CMV-enhanced green fluorescent protein (EGFP) cassette, creating the plasmid pAdTrack-*ATXN2*US. The resultant plasmid was then modified by adding *ATXN2* cDNAs with varying CAG repeat lengths and bovine growth hormone polyadenylation (BGH PolyA) signal by acquiring inserts from pCMV-Flag-*ATXN2*(CAG)<sub>n</sub> plasmids by PCR using *NotI* primers ATX-Fwd (5'-TCAGCGGCCGAGCTCCTCGGAGTCCC-3') and BGH-Rev (5'-TTTGCGGCCGCTTCCCCAGCATGCCT GCTATTG-3'). The inserts were digested with *NotI* and ligated into *NotI* digested pAdTrack-*ATXN2*US to create the pAdTrack-*ATXN2*(CAG)<sub>n</sub> plasmids, expressing ataxin-2 C-terminally tagged with the Flag epitope. The pCMV-Flag-*ATXN2*(CAG)<sub>n</sub> plasmids were previously cloned by amplifying inserts from corresponding pEGFP-SCA2(CAG)<sub>n</sub> plasmids (45) using primers *HindIII*2-Fwd (5'-GGGAAGCTTATGCGCTCAGCGGCCGAGCTCC-3') and *Sall*-Rev (5'-AAAGTCGACCAACTGCTGTTGGTGGTGGGC TTG-3') and ligating the *HindIII/Sall* digested inserts into a pCMV-3Tag-8 vector (Stragagene) digested with the same two restriction enzymes. Plasmid sequences were verified by sequencing.

### Site-directed mutagenesis of pGL2-5A3

We identified a 26 bp region 75 bp upstream of the start codon important for supporting *ATXN2* expression and possessing predictions for binding by multiple TFs. Mutations in pGL2-5A3 in this region were accomplished by using the QuickChange Lightning Site-Directed Mutagenesis Kit (Stratagene). The mCGA mutation, a TCC→CGA mutation in the *ATXN2* promoter, was created using the mutagenesis oligonucleotides MutR1A (5'-CCGTCTGACCCCTCCGAC TCGAGGTAAAGAGTCCC-3') and MutR1B (5'-GGGACTC TTTACCTCGAGTCGGAGGGGTCAGACGG-3'). The D14 mutation, a 14 bp deletion in this region of the *ATXN2* promoter, was created using the mutagenesis oligonucleotides MutR2A (5'-CCGTCTGACCCCTCGAGTCCCTATCCGC-3') and MutR2B (5'-GCGGATAGGGACTCGAGGGGT CAGACGG-3'). Mutagenesis was accomplished following the vendor's protocol.

### TF expression plasmids

The expression plasmid for ETS1 was provided by Barbara Graves (University of Utah). To create an expression plasmid for ELF2, we ligated the ELF2 cDNA between the *BamHI* and *XbaI* sites of pcDNA3.1(+). The ELF2 cDNA was obtained by PCR using primers ELF2Bam-A

(5'-CAGCGGATCCATAAACATGGCGACGTCTC-3') and ELF2Xba-B (5'-GGAGCTTCTAGATTATTTCTCACATG TCACTAGT-3') using template pBluescript-ELF2. An insert for the dn-ETS1 fragment including ETS1 amino acids 307–441 (46) was obtained by PCR with primers ETS1DN-A (5'-CCAGGGATCCATGTATGTGCGGGACCGTGCTGAC-3') and ETS1DN-B (5'-AGTGCTCGAGTCACTCGTGGCATCT GGCTTGA-3') and ligated between the *Bam*HI and *Xho*I sites of pcDNA3.1/Hygro(+). (Invitrogen).

### Luciferase assays

HEK293 or SH-SY5Y neuroblastoma cells were grown in Dulbecco's Modified Eagle Medium with 10% fetal bovine serum and  $1 \times$  penicillin/streptomycin. Cells were transfected using Metafectene (Biontex Laboratories) or Xfect (Clontech). Transfections were conducted in triplicate wells of a 24-well plate and typically consisted of 125 ng of pGL2-5A3 plasmid (mutant or wild-type) and 40 ng of pRL-SV40 or pRL-TK (Promega). Dose-wise transfections including *ETS1* plasmids were balanced with an empty vector to ensure consistent total DNA quantities. Assays were performed in triplicate per transfection after 48 h transfection using the Dual-Glo Luciferase Assay System (Promega), recording relative light units (RLUs) from firefly luciferase and Renilla luciferase on a multimode plate reader (Beckman DT880). Values were reported as the mean  $\pm$  SD of the ratios of  $RLU_{\text{firefly}}/RLU_{\text{RLuc}}$  (referred to in the text as 'relative luciferase activity'), with  $n = 3$  transfections for the calculation of SD. Each experiment was repeated at least three times.

### Immunoblotting

Proteins were separated on precast polyacrylamide gels (Bio-Rad), transferred to Hybond (Amersham) and detected by ECL (Amersham). Antibodies included goat anti-luciferase (Rockland Immunochemicals),  $\beta$ -actin mAb (AC-40, Sigma), anti-ETS-1(C-4, Santa Cruz Biotechnology), anti-FLAG antibody (Sigma) and anti-GFP antibody (Invitrogen). Secondary antibodies were purchased from Jackson ImmunoResearch Laboratories.

### TF-binding site prediction

Predictions for TF-binding sites were made using MatInspector (Genomatix) (47) and TESS (48).

### Real-time PCR

Real-time PCR (qPCR) was conducted by the SYBR Green method with standard curves on the iCycler (Bio-Rad) in 96-well plates in quadruplicate. RNAs were isolated from 30 mg tissue using the RNeasy Kit (Qiagen). cDNAs were generated using the QuantiTect Reverse Transcription kit (Qiagen). Primers for *luc* were GL2luc-2F (5'-ATCCG GAAGCGACCAACGCC-3') and GL2luc-2R (5'-GTCCGGA AGACCTGCCACGC-3') (212 bp product, 60°C annealing temperature). Primers for mouse *ATXN2* were ATXN-m5a (5'-AAGATACAGACTCCAGTTATGCACGG-3') and ATXN-m6b (5'-GCTCCAGGTCCTTCTCCTTGTC-3') (96 bp

product, 60°C annealing temperature). Primers for human *ATXN2* were HAtxn2-fwd (5'-AAGATATGGACTCCAGTTA TGCAAA-3') and HAtxn2-rev (5'-CAAAGCCTCAAGTT CCTCAT-3') (143 bp product, 60°C annealing temperature). Primers for Renilla luciferase were RenA (5'-GGCCAT GATTGGGGTGCTTGTT-3') and RenB (5'-CGGGATTC ACGAGGCCATGA-3') (321 bp product, 55°C annealing temperature). Reactions were 20  $\mu$ l consisting of 15 ng of cDNA, 2  $\mu$ l of each primer (0.3  $\mu$ M final) and 10  $\mu$ l of SYBR Green Master Mix (Bio-Rad). Cycling parameters included a 95°C denaturation for 10 s, an incubation at the annealing temperature for 20 s and a 40 s incubation at 72°C. Each plate included a standard curve using cerebellar RNA prepared from multiple pGL2-5A3 transgenic mice. Single amplicons were verified by denaturation analysis and gel electrophoresis.

### Electromobility shift assays

Nuclear extracts were prepared using the NE-PER Nuclear and Cytoplasmic Extraction Kit (Pierce) from HEK293 or SH-SY5Y cells, following the vendor's protocol. Protein concentrations were determined using the Bio-Rad Protein Assay (Bio-Rad). EMSA was performed using the non-radioactive LightShift Chemiluminescent EMSA kit (Pierce) following the vendor's protocol starting with 3  $\mu$ g nuclear protein per assay. For ETS and STAT EMSA supershift experiments, the oligonucleotide probe sets included WT-sense (5'-TC CGACTTCCGGTAAAGAGTC-3') and WT-antisense (5'-GACTCTTTACCGGAAGTCGGA-3'), mCGA-sense (5'-TCCGA CTGAGGTAAAGAGTC-3') and mCGA-antisense (5'-GACTCTTTACCTCGAGTCGGA-3') and RANDOM-sense (5'-CTAGCAGCTGATCTCAGCTGA-3') and RANDOM-antisense (5'-TCAGCTGAGATCAGCTGCTAG-3'). For forkhead EMSA supershift experiments, the oligonucleotide probe sets included SO7-A (5'-ACCCCTCCGACTTCCGGTAA AGAGTCCCTA-3') and SO7-B (5'-TAGGGACTCTTTA CCGGAAGTCGGAGGGGT-3') and SO7m-A (5'-ACCC TCCGACTTCCGGTATTCCTCCCTA-3') and SO7m-B (5'-TAGGGAGTGAATACCGGAAGTCGGAGGGGT-3'). Oligonucleotides were synthesized by the University of Utah Sequencing Core either unlabeled or biotinylated on the 3' end. Annealing was accomplished by mixing sense and antisense oligonucleotides of each set at equimolar concentrations in annealing buffer (0.1 mM Tris-HCl, pH 8), heating to 95°C in a heat block, then allowing the block to slowly cool to room temperature over 60 min. EMSAs were 20  $\mu$ l consisting of  $1 \times$  reaction buffer, 5  $\mu$ g/ $\mu$ l poly(dI.dC), 10% glycerol, 2.5 mM  $MgCl_2$ , 25 mM KCl, 1 mM ethylenediaminetetraacetic acid and 20 fmol biotinylated probe. Supershift assays were accomplished by including 4  $\mu$ g antibody. Antibodies used for supershift assays included ETS-1(C-4)X, NERF(C-20)X, GABP $\alpha$ (C-20)X, ELF1(C-20)X, FKHL1(N-16)X, FKHL(H-128)X, STAT1 p84/p91(E-23)X, STAT2(C-20)X, STAT3(C-20)X and STAT5(C-17)X (Santa Cruz Biotechnology).

### Chromatin immunoprecipitation PCR

Chromatin was prepared using the Pierce Chromatin Prep Module (Pierce). Formaldehyde was added to the cells ( $2 \times 10^6$  cells/ChIP reaction) at a final concentration of 1%. Cells

were incubated at room temperature for 10 min. Then excess formaldehyde was neutralized by the addition of glycine (1×) and incubating at room temperature for 5 min. After washing twice with cold phosphate buffered saline (PBS), the cells were scraped into 1 ml of cold PBS plus 1 × Halt Cocktail. The cells were pelleted and then suspended in 100 µl of lysis buffer 1 plus 1 × Halt Cocktail. After incubating 10 min on ice, the sample was centrifuged at 9000g and the supernatant was discarded. Isolated nuclei were suspended in MNase Digestion Buffer containing 1 mM dithiothreitol. Cross-linked DNA was fragmented by Micrococcal Nuclease (10 U/µl) at 37°C for 15 min, and the reaction was stopped by the addition of MNase Stop Solution. The solution was then centrifuged at 9000g to recover the nuclei. Digested chromatin was resuspended in 50 µl of lysis buffer 2 plus 1 × Halt Cocktail and incubated on ice for 15 min. The sample was centrifuged at 900g and chromatin was recovered in supernatant. ChIP assay was carried out using Pierce Agarose ChIP Kit (Pierce). Diluted chromatin was incubated with 10 µl anti-ETS1 antibody (diluted to 1 mg/ml, Santa Cruz ETS-1(C-4)X), 10 µl normal rabbit IgG (1 mg/ml stock) or 10 µl antibody diluent, at 4°C overnight. Complexes were column purified using protein A/G-agarose (incubated at 4°C for 1 h) with multiple washes using IP wash buffer 2 and IP wash buffer 3. Samples were eluted in 150 µl of IP elution buffer for 40 min at 65°C with intermittent vortexing. Reverse cross-linked DNAs were purified by using a kit provided DNA Clean-up Columns. Two microliters of each of the purified DNA was used as a template for 30 cycles of PCR amplification using primers C-ATXN2A3 (5'-AGGAAGGCGGATCCGGGTAG-3') and C-ATXN2B2 (5'-GGGAGCGGAGGTGCGGATAG-3'). ChIP reactions were also evaluated by qPCR and binding ratios were calculated as (starting quantity for anti-ETS1)/(starting quantity for rabbit IgG).

### ETS1 knockdown

*ETS1* knockdown was accomplished using an *ETS1* shRNA-8236 expression plasmid provided by Barbara Graves known to the knockdown expression of both the 42 and 51 kDa *ETS1* splicing isoforms (referred to as 'A' in 49). The sequence targeted in *ETS1* is 5'-AGGTGTAGACTTCAGAAG-3'. A control shRNA targeting EGFP was also used (#RHS4459, Open Biosystems).

### Transgenic mice

We made transgenic mice using an *ATXN2-luc* fragment excised from pGL2-5A3 with *HpaI* and *AfeI*. The mice were created by pronuclear injection at the University of Utah Transgenic Mouse Core using C57BL/6J mice. Founder screening was accomplished by tail-tip PCR identifying eight founders. Each founder was back-crossed to wild-type mice and one F1 littermate from each line was evaluated by assaying for luciferase. To do so, we homogenized ~100 mg cerebellum in PBS, added an equal volume of Bright-Glo Luciferase Assay Reagent (Promega) and determined RLU on a multimode plate reader (Beckman DT880). We saved two transgenic lines with the highest *ATXN2-luc* expression

determined as RLU/mg cerebellum tissue. Lines were designated L74 and L75. Only data on the highest expressing line L75 are presented.

### Optical imaging

Optical imaging was performed using a Xenogen IVIS 100 imaging system. Mice were IP injected with 50 mg/kg of D-luciferin diluted in PBS (10 µl/g body weight of 5 mg/ml D-luciferin). After 5 min, mice were anesthetized with isoflurane and were either directly imaged or tissues were excised for imaging. Imaging was conducted for a period of 1 min at 10 min after injection of substrate. Imaging of whole mice was preceded by hair removal using Nair.

### IF labeling

The OB from C57Bl/6 mice was frozen mounted in OCT and sectioned in 18 µm sections on a cryostat. Sections were fixed in 4% paraformaldehyde for 1 h then were permeabilized and blocked in blocking buffer (PBS, 0.3% Triton X-100, 5% milk) for 5 h. For labeling of HEK293 cells, cells transfected with *ETS1* were grown on coverslips 48 h then fixed in 4% paraformaldehyde for 20 min. The primary antibody in antibody diluent (PBS, 0.05% Triton X-100, 5% milk) was incubated on tissues overnight at 4°C. Primary antibodies were polyclonal rabbit anti-ataxin-2-1080 (5 µg/ml), Atxn-2 mAb (BD Transduction Laboratories 611378, 2.5 µg/ml), interneuron marker antibody GAD65/67 (SC-75-13, Santa Cruz Biotechnology, 4 µg/ml) and polyclonal rabbit anti-ETS-1(C-4, Santa Cruz Biotechnology, 1:10:000). Cells were washed in wash buffer (PBS, 0.01% Triton X-100, 1% milk) then incubated with secondary antibodies (1 µg/ml) diluted in secondary antibody diluent (PBS, 3% normal goat serum) for 2 h at room temperature. Secondary antibodies were anti-rabbit-Dylight 488 (611-741-127), anti-mouse-Dylight 549 (610-742-124) and anti-goat-549 Dylight (605-742-125) (Rockland Inc., Gilbertsville, PA, USA). Cells were washed in wash buffer, incubated in 1 µg/ml 4',6-diamidino-2-phenylindole (DAPI)/PBS for 5 min and mounted using Prolong Gold (Invitrogen). Standard fluorescent images were collected using a Nikon C1 fluorescent microscope (NIS Elements software) with a 488/561 nm filter set (for DyLight 488 and 549) or 408 nm filter (for DAPI) and a 408/488/561 dichroic mirror.

### Statistical analysis

Unpaired two-tailed *t*-tests were conducted for selected pairwise comparisons. When multiple tests were performed, it was accomplished by one-way ANOVA and we reported probabilities from Bonferroni post-tests.

### SUPPLEMENTARY MATERIAL

Supplementary Material is available at *HMG* online.

## ACKNOWLEDGEMENTS

We thank Barbara Graves for contributing to the interpretation of data and for providing ETS1 expression plasmid and rat prolactin minimal promoter reporter plasmid rPrl-luc, and Mary Lucero for interpretations on OB IHC. We also thank Stephen Lessnick for providing access to the Xenogen IVIS100 instrument for *in vivo* imaging of *ATXN2-luc* in mice. We thank Karla Figueroa, Seth Christensen, Patrick Gordon and Sharan Paul for their contributions.

*Conflict of Interest statement.* None declared.

## FUNDING

This work was supported by National Institutes of Health (R01NS033123 to S.M.P. and RC4NS073009 to S.M.P. and D.R.S.).

## REFERENCES

- Pulst, S.M. (2003) Inherited ataxias: an introduction. In Pulst, S.M. (ed.), *Genetics of Movement Disorders*. Elsevier, Inc., Amsterdam, pp. 19–34.
- Kim, J.M., Hong, S., Kim, G.P., Choi, Y.J., Kim, Y.K., Park, S.S., Kim, S.E. and Jeon, B.S. (2007) Importance of low-range CAG expansion and CAA interruption in SCA2 Parkinsonism. *Arch. Neurol.*, **64**, 1510–1518.
- Ross, O.A., Rutherford, N.J., Baker, M., Soto-Ortolaza, A.I., Carrasquillo, M.M., DeJesus-Hernandez, M., Adamson, J., Li, M., Volkening, K., Finger, E. *et al.* (2011) Ataxin-2 repeat-length variation and neurodegeneration. *Hum. Mol. Genet.*, **20**, 3207–3212.
- Corrado, L., Mazzini, L., Oggioni, G.D., Luciano, B., Godi, M., Brusco, A. and D'Alfonso, S. (2011) ATXN-2 CAG repeat expansions are interrupted in ALS patients. *Hum. Genet.*, **130**, 575–580.
- Elden, A.C., Kim, H.J., Hart, M.P., Chen-Plotkin, A.S., Johnson, B.S., Fang, X., Armakola, M., Geser, F., Greene, R., Lu, M.M. *et al.* (2010) Ataxin-2 intermediate-length polyglutamine expansions are associated with increased risk for ALS. *Nature*, **466**, 1069–1075.
- Van Damme, P., Veldink, J.H., van Blitterswijk, M., Corveleyn, A., van Vught, P.W., Thijs, V., Dubois, B., Matthijs, G., van den Berg, L.H. and Robberecht, W. (2011) Expanded ATXN2 CAG repeat size in ALS identifies genetic overlap between ALS and SCA2. *Neurology*, **76**, 2066–2072.
- Lajoie, P. and Snapp, E.L. (2011) Formation and toxicity of soluble polyglutamine oligomers in living cells. *PLoS One*, **5**, e15245.
- Huynh, D.P., Del Bigio, M.R., Ho, D.H. and Pulst, S.M. (1999) Expression of ataxin-2 in brains from normal individuals and patients with Alzheimer's disease and spinocerebellar ataxia 2. *Ann. Neurol.*, **45**, 232–241.
- Huynh, D.P., Yang, H.T., Vakharia, H., Nguyen, D. and Pulst, S.M. (2003) Expansion of the polyQ repeat in ataxin-2 alters its Golgi localization, disrupts the Golgi complex and causes cell death. *Hum. Mol. Genet.*, **12**, 1485–1496.
- Duvick, L., Barnes, J., Ebner, B., Agrawal, S., Andresen, M., Lim, J., Giesler, G.J., Zoghbi, H.Y. and Orr, H.T. (2010) SCA1-like disease in mice expressing wild-type ataxin-1 with a serine to aspartic acid replacement at residue 776. *Neuron*, **67**, 929–935.
- Yamanaka, T. and Nukina, N. (2010) Transcription factor sequestration by polyglutamine proteins. *Methods Mol. Biol.*, **648**, 215–229.
- Koshy, B., Matilla, T., Burrell, E.N., Merry, D.E., Fischbeck, K.H., Orr, H.T. and Zoghbi, H.Y. (1996) Spinocerebellar ataxia type-1 and spinobulbar muscular atrophy gene products interact with glyceraldehyde-3-phosphate dehydrogenase. *Hum. Mol. Genet.*, **5**, 1311–1318.
- Burke, J.R., Enghild, J.J., Martin, M.E., Jou, Y.S., Myers, R.M., Roses, A.D., Vance, J.M. and Strittmatter, W.J. (1996) Huntingtin and DRPLA proteins selectively interact with the enzyme GAPDH. *Nat. Med.*, **2**, 347–350.
- Nonhoff, U., Ralser, M., Welzel, F., Piccini, I., Balzereit, D., Yaspo, M.L., Lehrach, H. and Krobisch, S. (2007) Ataxin-2 interacts with the DEAD/H-box RNA helicase DDX6 and interferes with P-bodies and stress granules. *Mol. Biol. Cell*, **18**, 1385–1396.
- Shibata, H., Huynh, D.P. and Pulst, S.M. (2000) A novel protein with RNA-binding motifs interacts with ataxin-2. *Hum. Mol. Genet.*, **9**, 1303–1313.
- Ciosk, R., DePalma, M. and Priess, J.R. (2004) ATX-2, the *C. elegans* ortholog of ataxin 2, functions in translational regulation in the germline. *Development*, **131**, 4831–4841.
- Satterfield, T.F. and Pallanck, L.J. (2006) Ataxin-2 and its *Drosophila* homolog, ATX2, physically assemble with polyribosomes. *Hum. Mol. Genet.*, **15**, 2523–2532.
- Nonis, D., Schmidt, M.H., van de Loo, S., Eich, F., Dikic, I., Nowock, J. and Auburger, G. (2008) Ataxin-2 associates with the endocytosis complex and affects EGF receptor trafficking. *Cell Signal.*, **20**, 1725–1739.
- Liu, J., Tang, T.S., Tu, H., Nelson, O., Herndon, E., Huynh, D.P., Pulst, S.M. and Bezprozvanny, I. (2009) Deranged calcium signaling and neurodegeneration in spinocerebellar ataxia type 2. *J. Neurosci.*, **29**, 9148–9162.
- Pulst, S.M., Santos, N., Wang, D., Yang, H., Huynh, D., Velazquez, L. and Figueroa, K.P. (2005) Spinocerebellar ataxia type 2: polyQ repeat variation in the CACNA1A calcium channel modifies age of onset. *Brain*, **128**, 2297–2303.
- Yamamoto, A., Lucas, J.J. and Hen, R. (2000) Reversal of neuropathology and motor dysfunction in a conditional model of Huntington's disease. *Cell*, **101**, 57–66.
- Zu, T., Duvick, L.A., Kaytor, M.D., Berlinger, M.S., Zoghbi, H.Y., Clark, H.B. and Orr, H.T. (2004) Recovery from polyglutamine-induced neurodegeneration in conditional SCA1 transgenic mice. *J. Neurosci.*, **24**, 8853–8861.
- Boy, J., Schmidt, T., Wolburg, H., Mack, A., Nuber, S., Bottcher, M., Schmitt, I., Holzmann, C., Zimmermann, F., Servadio, A. *et al.* (2009) Reversibility of symptoms in a conditional mouse model of spinocerebellar ataxia type 3. *Hum. Mol. Genet.*, **18**, 4282–4295.
- Alves, S., Nascimento-Ferreira, I., Dufour, N., Hassig, R., Auresan, G., Nobrega, C., Brouillet, E., Hantraye, P., Pedrosa de Lima, M.C., Deglon, N. *et al.* (2010) Silencing ataxin-3 mitigates degeneration in a rat model of Machado-Joseph disease: no role for wild-type ataxin-3? *Hum. Mol. Genet.*, **19**, 2380–2394.
- Kiehl, T.R., Nechiporuk, A., Figueroa, K.P., Keating, M.T., Huynh, D.P. and Pulst, S.M. (2006) Generation and characterization of Sca2 (ataxin-2) knockout mice. *Biochem. Biophys. Res. Commun.*, **339**, 17–24.
- Aguiar, J., Santurlidis, S., Nowok, J., Alexander, C., Rudnicki, D., Gispert, S., Schulz, W. and Auburger, G. (1999) Identification of the physiological promoter for spinocerebellar ataxia 2 gene reveals a CpG island for promoter activity situated into the exon 1 of this gene and provides data about the origin of the nonmethylated state of these types of islands. *Biochem. Biophys. Res. Commun.*, **254**, 315–318.
- Hallen, L., Klein, H., Stoschek, C., Wehrmeyer, S., Nonhoff, U., Ralser, M., Wilde, J., Rohr, C., Schweiger, M.R., Zatloukal, K. *et al.* (2011) The KRAB-containing zinc-finger transcriptional regulator ZBRK1 activates SCA2 gene transcription through direct interaction with its gene product, ataxin-2. *Hum. Mol. Genet.*, **20**, 104–114.
- Hollenhorst, P.C., Shah, A.A., Hopkins, C. and Graves, B.J. (2007) Genome-wide analyses reveal properties of redundant and specific promoter occupancy within the ETS gene family. *Genes. Dev.*, **21**, 1882–1894.
- Crespo-Barreto, J., Fryer, J.D., Shaw, C.A., Orr, H.T. and Zoghbi, H.Y. (2010) Partial loss of ataxin-1 function contributes to transcriptional dysregulation in spinocerebellar ataxia type 1 pathogenesis. *PLoS Genet.*, **6**, e1001021.
- Allen Mouse Brain Atlas [Internet]. Allen Institute for Brain Science, Seattle, WA, 2009. <http://mouse.brain-map.org>.
- Lein, E.S., Hawrylycz, M.J., Ao, N., Ayres, M., Bensinger, A., Bernard, A., Boe, A.F., Boguski, M.S., Brockway, K.S., Byrnes, E.J. *et al.* (2007) Genome-wide atlas of gene expression in the adult mouse brain. *Nature*, **445**, 168–176.
- Lastres-Becker, I., Brodesser, S., Lutjohann, D., Azizov, M., Buchmann, J., Hintermann, E., Sandhoff, K., Schurmann, A., Nowock, J. and Auburger, G. (2008) Insulin receptor and lipid metabolism pathology in ataxin-2 knock-out mice. *Hum. Mol. Genet.*, **17**, 1465–1481.

33. McCann, C., Holohan, E.E., Das, S., Dervan, A., Larkin, A., Lee, J.A., Rodrigues, V., Parker, R. and Ramaswami, M. (2011) The Ataxin-2 protein is required for microRNA function and synapse-specific long-term olfactory habituation. *Proc. Natl Acad. Sci. USA*, **108**, E655–E662.
34. Velazquez-Perez, L., Fernandez-Ruiz, J., Diaz, R., Gonzalez, R.P., Ochoa, N.C., Cruz, G.S., Mederos, L.E., Gongora, E.M., Hudson, R. and Drucker-Colin, R. (2006) Spinocerebellar ataxia type 2 olfactory impairment shows a pattern similar to other major neurodegenerative diseases. *J. Neurol.*, **253**, 1165–1169.
35. Laffita-Mesa, J.M., Bauer, P.O., Kouri, V., Pena Serrano, L., Roskams, J., Almaguer Gotay, D., Montes Brown, J.C., Martinez Rodriguez, P.A., Gonzalez-Zaldivar, Y., Almaguer Mederos, L. *et al.* (2011) Epigenetics DNA methylation in the core ataxin-2 gene promoter: novel physiological and pathological implications. *Hum. Genet.*, **131**, 625–638.
36. Zu, T., Gibbens, B., Doty, N.S., Gomes-Pereira, M., Huguet, A., Stone, M.D., Margolis, J., Peterson, M., Markowski, T.W., Ingram, M.A. *et al.* (2011) Non-ATG-initiated translation directed by microsatellite expansions. *Proc. Natl Acad. Sci. USA*, **108**, 260–265.
37. Broda, M., Kierzek, E., Gdaniec, Z., Kulinski, T. and Kierzek, R. (2005) Thermodynamic stability of RNA structures formed by CNG trinucleotide repeats. Implication for prediction of RNA structure. *Biochemistry*, **44**, 10873–10882.
38. Dansithong, W., Wolf, C.M., Sarkar, P., Paul, S., Chiang, A., Holt, I., Morris, G.E., Branco, D., Sherwood, M.C., Comai, L. *et al.* (2008) Cytoplasmic CUG RNA foci are insufficient to elicit key DMI features. *PLoS One*, **3**, e3968.
39. Sobczak, K. and Krzyzosiak, W.J. (2005) CAG repeats containing CAA interruptions form branched hairpin structures in spinocerebellar ataxia type 2 transcripts. *J. Biol. Chem.*, **280**, 3898–3910.
40. Gerhauser, I., Alldinger, S., Ulrich, R. and Baumgartner, W. (2005) Spatio-temporal expression of immediate early genes in the central nervous system of SJL/J mice. *Int. J. Dev. Neurosci.*, **23**, 637–649.
41. Miyake, T., Aoki, M., Osako, M.K., Shimamura, M., Nakagami, H. and Morishita, R. (2011) Systemic administration of ribbon-type decoy oligodeoxynucleotide against nuclear factor kappaB and ets prevents abdominal aortic aneurysm in rat model. *Mol. Ther.*, **19**, 181–187.
42. Souissi, I., Najjar, I., Ah-Koon, L., Schischmanoff, P.O., Lesage, D., Le Coquil, S., Roger, C., Dusanter-Fourt, I., Varin-Blank, N., Cao, A. *et al.* (2011) A STAT3-decoy oligonucleotide induces cell death in a human colorectal carcinoma cell line by blocking nuclear transfer of STAT3 and STAT3-bound NF-kappaB. *BMC Cell Biol.*, **12**, 14.
43. Alexander, J.H., Hafley, G., Harrington, R.A., Peterson, E.D., Ferguson, T.B. Jr, Lorenz, T.J., Goyal, A., Gibson, M., Mack, M.J., Gennevois, D. *et al.* (2005) Efficacy and safety of edifoligide, an E2F transcription factor decoy, for prevention of vein graft failure following coronary artery bypass graft surgery: PREVENT IV: a randomized controlled trial. *JAMA*, **294**, 2446–2454.
44. Ng, H., Pulst, S.M. and Huynh, D.P. (2007) Ataxin-2 mediated cell death is dependent on domains downstream of the polyQ repeat. *Exp. Neurol.*, **208**, 207–215.
45. Huynh, D.P., Figueroa, K., Hoang, N. and Pulst, S.M. (2000) Nuclear localization or inclusion body formation of ataxin-2 are not necessary for SCA2 pathogenesis in mouse or human. *Nat. Genet.*, **26**, 44–50.
46. Holterman, C.E., Franovic, A., Payette, J. and Lee, S. (2010) ETS-1 oncogenic activity mediated by transforming growth factor alpha. *Cancer Res.*, **70**, 730–740.
47. Quandt, K., Frech, K., Karas, H., Wingender, E. and Werner, T. (1995) MatInd and MatInspector: new fast and versatile tools for detection of consensus matches in nucleotide sequence data. *Nucleic Acids Res.*, **23**, 4878–4884.
48. Schug, J. (2008) Using TESS to predict transcription factor binding sites in DNA sequence. *Curr. Protoc. Bioinformatics.*, **Chapter 2**, Unit 2.6.
49. Hollenhorst, P.C., Chandler, K.J., Poulsen, R.L., Johnson, W.E., Speck, N.A. and Graves, B.J. (2009) DNA specificity determinants associate with distinct transcription factor functions. *PLoS Genet.*, **5**, e1000778.